



HAL
open science

Spectral convergence of the generalized Polynomial Chaos reduced model obtained from the uncertain linear Boltzmann equation

Gaël Poëtte

► **To cite this version:**

Gaël Poëtte. Spectral convergence of the generalized Polynomial Chaos reduced model obtained from the uncertain linear Boltzmann equation. *Mathematics and Computers in Simulation*, 2020. hal-02090593v2

HAL Id: hal-02090593

<https://hal.science/hal-02090593v2>

Submitted on 3 Apr 2020

HAL is a multi-disciplinary open access archive for the deposit and dissemination of scientific research documents, whether they are published or not. The documents may come from teaching and research institutions in France or abroad, or from public or private research centers.

L'archive ouverte pluridisciplinaire **HAL**, est destinée au dépôt et à la diffusion de documents scientifiques de niveau recherche, publiés ou non, émanant des établissements d'enseignement et de recherche français ou étrangers, des laboratoires publics ou privés.

Spectral convergence of the generalized Polynomial Chaos reduced model obtained from the uncertain linear Boltzmann equation

Gaël Poëtte*

April 3, 2020

Abstract

In this paper, we consider the linear Boltzmann equation subject to uncertainties in the initial conditions and matter parameters (cross-sections/opacities). In order to solve the underlying uncertain systems, we rely on moment theory and the construction of hierarchical moment models in the framework of parametric polynomial approximations. Such model is commonly called a generalised Polynomial Chaos (gPC) reduced model. In this paper, we prove the spectral convergence of the hierarchy of reduced model parametered by P (polynomial order) obtained from the uncertain linear Boltzmann equation.

1 Introduction

In this paper, we are interested in the linear Boltzmann equation recalled below

$$\begin{cases} \partial_t u(\mathbf{x}, t, \mathbf{v}) + \mathbf{v} \cdot \nabla_{\mathbf{x}} u(\mathbf{x}, t, \mathbf{v}) = -v\sigma_t(\mathbf{x}, t, \mathbf{v})u(\mathbf{x}, t, \mathbf{v}) + \int v\sigma_s(\mathbf{x}, t, \mathbf{v}, \mathbf{v}')u(\mathbf{x}, t, \mathbf{v}') d\mathbf{v}', \\ u(\mathbf{x}, 0, \mathbf{v}) = u_0(\mathbf{x}, \mathbf{v}). \end{cases} \quad (1)$$

It models the time-dependent problem of particle transport in a collisional media. We suppose transport to be driven by the linear Boltzmann equation (1) for particles having position $\mathbf{x} \in \mathcal{D} \subset \mathbb{R}^3$, velocity $\mathbf{v} \in \mathcal{V} \subset \mathbb{R}^3$, at time $t \in [0, T] \subset \mathbb{R}^+$ and where the quantity $u(\mathbf{x}, t, \mathbf{v}) \in \Omega \subset \mathbb{R}^+$ is the density of presence of the particles at $(\mathbf{x}, t, \mathbf{v})$. In (1), we introduced the notation $|\mathbf{v}| = v$ to denote the norm of the velocity \mathbf{v} . Later on, we may also use $\omega = \frac{\mathbf{v}}{v}$, the unitary vector for the direction of the particles. Equation (1) must come with proper boundary conditions for wellposedness [35] but we omit them for the sake of conciseness. In other words, the Cauchy problem (1) is valid in an infinite medium and regular solutions can be expected [27, 9]. The left hand side of (1) will be hinted at as the *streaming* counterpart of (1) whereas its right hand side will be called the *collisional* one. The above equation is linear and can be used to model the behaviour of particles interacting with a *background* media. A solution of (1) is called a deterministic solution. The interaction of particles with matter is described through the macroscopic total $\sigma_t(\mathbf{x}, t, \mathbf{v})$ and scattering $\sigma_s(\mathbf{x}, t, \mathbf{v}, \mathbf{v}')$ cross-sections. They express the probability for a particle to interact with the medium (to be absorbed, scattered, to encounter a particular reaction etc.). The cross-sections, in a sense, contain all the physics (which is kind of hidden in this paper): they can be related to other coupled physics such as reactive flows, isotopic depletion [17] in neutronics, temperature dependence for photonics [51] or media subject to material motion [64] (neutronics, photonics, plasma physics). Those physics may communicate uncertainties to the particle transport *via* the cross-sections. Taking into account uncertainties in the cross-sections

*CEA, CESTA, DAM, F-33114 Le Barp, France

2 The gPC reduced model obtained from the uncertain linear Boltzmann equation (4)

The standard method to construct a gPC based reduced model is the following. We first define the set of k integrable uncertain functions

$$L_{\Theta}^k = \left\{ \text{measurable functions } X \mapsto f(X) \text{ such that } \int_{\Theta} |f(\xi)|^k d\mathcal{P}_X(\xi) < \infty \right\}. \quad (5)$$

In particular, we focus on functions of $L^2(\Theta)$. Under very general conditions [19, 21], there exists a countable family of polynomials $(\phi_q)_{q \in \mathbb{N}}$ which are orthonormal with respect to the scalar product defined by $d\mathcal{P}_X$. In other words, we have

$$\int_{\Theta} \phi_p(\xi) \phi_q(\xi) d\mathcal{P}_X(\xi) = \int \phi_p \phi_q d\mathcal{P}_X = \delta_{pq}, \forall (p, q) \in \mathbb{N}^2.$$

In practice, in the above expression, the basis must be truncated up to certain orders $(p_i)_{i \in \{1, \dots, Q\}}$ which may depend on the directions $(X_i)_{i \in \{1, \dots, Q\}}$. Assume that $\forall i \in \{1, \dots, Q\}$, $p_i = p_{1D}$, then the total number of polynomial coefficients, abusively called the polynomial order later on, is $P = P(p_{1D}, Q) = (p_{1D} + 1)^Q$. It exhibits an exponential growth with both p_{1D} and Q . This is commonly called *the curse of dimensionality* [5, 13]. As a consequence, the reduced models described in this paper, in practice, can only be applied to a moderate number of uncertain parameters ($Q \sim 10$). The multivariate polynomial basis is built by tensorization of one-dimensional polynomial basis in every stochastic direction $(X_i)_{i \in \{1, \dots, Q\}}$. In the following sections, for conciseness in the notations, we map³ the set of polynomial indices $\mathcal{A}^{p_{1D}, Q} = \{(k_1, \dots, k_Q) | \forall i \in \{1, \dots, Q\}, k_i \leq p_{1D}\}$ into $\{0, \dots, P\}$ to build the tensorized basis $(\phi_k(X) = \prod_{i=1}^Q \phi_{k_i}^{X_i}(X_i))_{k \in \{0, \dots, P\}}$. In the previous expression, $\forall i \in \{1, \dots, Q\}$, the basis $(\phi_k^{X_i})_{k \in \{0, \dots, p_{1D}\}}$ is a one-dimensional polynomial basis orthonormal with respect to $d\mathcal{P}_{X_i}$. When P grows, we assume it grows because the one-dimensional polynomial orders p_{1D} grow.

At fixed $t \in [0, T] \subset \mathbb{R}^+$, $\mathbf{x} \in \mathcal{D} \subset \mathbb{R}^3$ and $\mathbf{v} \in \mathcal{V} \subset \mathbb{R}^3$, it is natural to look for an approximation of the solution u in the subspace $(\phi_k)_{k \in \{0, \dots, P\}}$ generated by the first $P + 1$ polynomials of $(\phi_k)_{k \in \mathbb{N}}$. It is immediate to show that

$$u^P = \sum_{q=0}^P u_q \phi_q \text{ with } u_q = \int u \phi_q d\mathcal{P}_X, \quad (6)$$

is such that

$$\int_{\Theta} (u - u^P)^2 d\mathcal{P}_X \leq \int_{\Theta} (u - v^P)^2 d\mathcal{P}_X, \forall v^P \in (\phi_k)_{k \in \{0, \dots, P\}}.$$

In other words, expansion (6) is the best one among all possible trials in $(\phi_k)_{k \in \{0, \dots, P\}}$ with respect to the L_{Θ}^2 norm. In order to compute the coefficients $(u_q)_{q \in \{0, \dots, P\}}$, one can use the fact that u is the solution of an integro-differential equation with operators applying to t , \mathbf{x} and \mathbf{v} . The gPC methodology consists in developing the unknown u of (4) on the polynomial basis

$$u^P(\mathbf{x}, t, \mathbf{v}, X) = \sum_{q=0}^P u_q(\mathbf{x}, t, \mathbf{v}) \phi_q(X), \quad (7)$$

and look for compatibility conditions on the coefficients $(u_k)_{k \in \{0, \dots, P\}}$ for u^P to be a good approximation of u . This is usually done by plugging (7) into (4) and by taking the moments of (4) against each orthonormal components $(\phi_q)_{q \in \{0, \dots, P\}}$. The reader interested in efficient resolutions for different physical applications is referred to [41, 42, 47, 37, 56, 14, 24, 31, 25, 44, 26, 29, 5, 7, 20, 65, 55, 23, 58,

³It is only a reenumeration.

32, 33, 34, 18]. One finally obtains the moment model

$$\left\{ \begin{array}{l} \forall q \text{ such that } 0 \leq q \leq P, \\ \partial_t u_q(\mathbf{x}, t, \mathbf{v}) + \mathbf{v} \cdot \nabla_{\mathbf{x}} u_q(\mathbf{x}, t, \mathbf{v}) = -v \int \left(\sigma_t(\mathbf{x}, t, \mathbf{v}, X) \sum_{k \leq p} u_k(\mathbf{x}, t, \mathbf{v}) \phi_k(X) \right) \phi_q(X) d\mathcal{P}_X \\ \quad + \iint v \left(\left(\sigma_s(\mathbf{x}, t, \mathbf{v}, \mathbf{v}', X) \sum_{k \leq p} u_k(\mathbf{x}, t, \mathbf{v}) \phi_k(X) \right) \phi_q(X) d\mathcal{P}_X \right) d\mathbf{v}', \\ u_q(\mathbf{x}, 0, \mathbf{v}) = u_{0,q}(\mathbf{x}, \mathbf{v}). \end{array} \right. \quad (8)$$

Since u is scalar, system (8) is a system of $(P + 1)$ equations. It is a closed system in the sense that it has exactly $(P + 1)$ equations and $(P + 1)$ unknowns. In the following sections, system (8) will also be referred as the P -truncated gPC reduced model of (1) with standard closure (7).

It is reasonable to expect that (8) is an accurate approximation of the uncertain initial problem for large $P \gg 1$ (cf. Cameron-Martin's Theorem [10] or some generalization [19]). In fact, for this system, fast convergence rate have been practically observed in [50]. This paper is complementary to [50] in the sense that we here demonstrate the fast convergence of the P -truncated reduced models instead of only observing it *via* numerical experiments. We will indeed prove spectral accuracy under very general hypothesis in the next section 3.

3 Proof of spectral accuracy of the gPC reduced model

In this section we prove a result of spectral accuracy for the P -truncated gPC reduced models of the uncertain linear Boltzmann equation (8). We use a comparison method between a general approximated solution and a smooth exact solution to establish this result. The idea is similar to what has been proved in [15] for the scalar uncertain Burgers' equation for early times except it is applied to the uncertain linear Boltzmann equation which admits smoother solutions [27, 28, 3].

Let us assume the exact solution is smooth with respect to all variables

$$u \in L^\infty(\mathcal{D} \times [0, T] \times \mathcal{V} \times \Theta) \cap L^\infty(\mathcal{D}_{\text{per}} \times [0, T] \times \mathcal{V}_b : H^k(\Theta)). \quad (9)$$

In the above definition, \mathcal{D}_{per} denotes a periodic spatial domain. Periodic boundary conditions are considered only for convenience, without loss of generality. Furthermore, \mathcal{V} is the space of velocities and \mathcal{V}_b recalls it is bounded (dealing with physical applications, the particles can not go beyond the speed of light for example). More generally, as we are interested in dealing with physical applications, it is reasonable considering the density of particle $u(\mathbf{x}, t, \mathbf{v}, X)$ is bounded $\forall (\mathbf{x}, t, \mathbf{v}, X) \in \mathcal{D} \times [0, T] \times \mathcal{V} \times \Theta$.

Finally, for all $k \in \mathbb{N}$ we have

$$H^k(\Theta) = \left\{ u \in L^2_\Theta \mid \int \sum_{l=0}^k (u^{(l)})^2 d\mathcal{P}_X < \infty \right\},$$

where $u^{(l)}$ denotes the l^{th} derivative of u with respect to the uncertain variable. In other words, for solution $u(\mathbf{x}, t, \mathbf{v}, X)$, we have $u^{(l)}(\mathbf{x}, t, \mathbf{v}, \xi) = \partial_\xi^l u(\mathbf{x}, t, \mathbf{v}, \xi)$.

The gPC reduced model of (1) of size $P + 1$ is (we drop the dependencies for convenience)

$$\begin{cases} \partial_t u_0 + \mathbf{v} \cdot \nabla_{\mathbf{x}} u_0 &= -v \int \left(\sigma_t \sum_{k \leq P} u_k \phi_k \right) \phi_0 d\mathcal{P}_X + v \iint \left(\left(\sigma_s \sum_{k \leq P} u_k \phi_k \right) \phi_0 d\mathcal{P}_X \right) d\mathbf{v}', \\ \dots & \dots \\ \partial_t u_P + \mathbf{v} \cdot \nabla_{\mathbf{x}} u_P &= -v \int \left(\sigma_t \sum_{k \leq P} u_k \phi_k \right) \phi_P d\mathcal{P}_X + v \iint \left(\left(\sigma_s \sum_{k \leq P} u_k \phi_k \right) \phi_P d\mathcal{P}_X \right) d\mathbf{v}'. \end{cases} \quad (10)$$

It is then possible to perform the scalar product $(u_0, \dots, u_P)^t \partial_t (u_0, \dots, u_P)$ to obtain an additional equation. Let us consider a smooth solution of (10), we get

$$\begin{aligned} \partial_t \frac{\sum_{r=0}^P u_r^2}{2} + \mathbf{v} \cdot \nabla_{\mathbf{x}} \frac{\sum_{r=0}^P u_r^2}{2} &= \\ -v \int \sum_{q=0}^P \left(\sigma_t \sum_{k=0}^P u_k \phi_k \right) u_q \phi_q d\mathcal{P}_X + v \iint \sum_{q=0}^P \left(\left(\sigma_s \sum_{k=0}^P u_k \phi_k \right) u_q \phi_q d\mathcal{P}_X \right) d\mathbf{v}'. \end{aligned} \quad (11)$$

After rearrangement of the collisional counterpart, it yields

$$\partial_t \sum_{r=0}^P \frac{u_r^2}{2} + \mathbf{v} \cdot \nabla_{\mathbf{x}} \sum_{r=0}^P \frac{u_r^2}{2} = -v \sum_{0 \leq k, q \leq P} \int \sigma_t u_k \phi_k u_q \phi_q d\mathcal{P}_X + \sum_{0 \leq k, q \leq P} v \iint \sigma_s u_k \phi_k u_q \phi_q d\mathcal{P}_X d\mathbf{v}'. \quad (12)$$

Let us introduce

$$\sigma_s(\mathbf{x}, t, \mathbf{v}, X) = \int \sigma_s(\mathbf{x}, t, \mathbf{v}, \mathbf{v}', X) d\mathbf{v}' \text{ and define } P_s(\mathbf{x}, t, \mathbf{v}, \mathbf{v}', X) = \frac{\sigma_s(\mathbf{x}, t, \mathbf{v}, \mathbf{v}', X)}{\sigma_s(\mathbf{x}, t, \mathbf{v}, X)}.$$

We have

$$\begin{aligned} P_s(\mathbf{x}, t, \mathbf{v}, \mathbf{v}', X) &> 0, \quad \forall (\mathbf{x}, t, \mathbf{v}, \mathbf{v}', X) \in \mathcal{D} \times [0, T] \times \mathcal{V}^2 \times \Theta, \\ \int P_s(\mathbf{x}, t, \mathbf{v}, \mathbf{v}', X) d\mathbf{v}' &= 1, \quad \forall (\mathbf{x}, t, \mathbf{v}, X) \in \mathcal{D} \times [0, T] \times \mathcal{V} \times \Theta. \end{aligned} \quad (13)$$

The difference $\sigma_a(\mathbf{x}, t, \mathbf{v}, X) = \sigma_t(\mathbf{x}, t, \mathbf{v}, X) - \sigma_s(\mathbf{x}, t, \mathbf{v}, X)$ corresponds to an absorption rate if positive, or a multiplication rate, if negative. We now suggested making few assumptions on the background media in which the particles are evolving.

Hypothesis 1 $\forall t \in [0, T], \forall \mathbf{x} \in \mathcal{D}_{per}, \forall \mathbf{v} \in \mathcal{V}_b \subset \mathbb{R}^3, \forall X \in \Theta$

$$|v\sigma_t(\mathbf{x}, t, \mathbf{v}, X)| < \Sigma_t, \quad |v\sigma_s(\mathbf{x}, t, \mathbf{v}, X)| < \Sigma_s.$$

In other words, we have

$$\|v\sigma_t\|_{L^\infty(\mathcal{I} \times \Theta)} = \Sigma_t < \infty, \quad \|v\sigma_s\|_{L^\infty(\mathcal{I} \times \Theta)} = \Sigma_s < \infty. \quad (14)$$

The above hypothesis expresses the fact we consider a background media leading to a finite number of collisions (term $v\sigma_t$) for every interval of times $[0, T]$ together with a finite multiplication rate (term relative to $v\sigma_s$) in $[0, T]$.

Remark 3.1 Note that the above boundedness hypothesis 1 forbids modeling σ_t, σ_s by unbounded (for example gaussian) random variables. The same remark applies to condition (9) and u_0 . This comes from a will to ensure positivity and finiteness of those quantities which are primary data and are always positive and finite (not only positive and finite with probability one). Of course, nothing prevents from using unbounded random variables X to model u_0, σ_s, σ_t if the transformed random variables $X \rightarrow u_0(\mathbf{x}, t, \mathbf{v}, X), X \rightarrow \sigma_t(\mathbf{x}, t, \mathbf{v}, X)$ and $X \rightarrow \sigma_s(\mathbf{x}, t, \mathbf{v}, \mathbf{v}', X)$ remain bounded $\forall (\mathbf{x}, t, \mathbf{v}, \mathbf{v}') \in \mathcal{D} \times [0, T] \times \mathcal{V}^2$.

Now, let us integrate (12) with respect to $\mathbf{x}, t, \mathbf{v}$ on $\mathcal{D}_{per} \times [0, T] \times \mathcal{V}_b$, and use the above majorations. Let us define for convenience (we here introduce equivalent notations which will be useful later on)

$$\begin{aligned}
\|u^P(t)\|_{L^2(\mathcal{D}_{per} \times \mathcal{V}_b \times \Theta)}^2 &= \|u^P(t)\|_{L^2(\mathcal{I} \times \Theta)}^2, \\
&= \iint \sum_{r=0}^P u_r^2(\mathbf{x}, t, \mathbf{v}) \, d\mathbf{x} \, d\mathbf{v}, \\
&= \iiint \sum_{r=0}^P (u_r(\mathbf{x}, t, \mathbf{v}) \phi_r(\xi))^2 \, d\mathbf{x} \, d\mathbf{v} \, d\mathcal{P}_X(\xi), \\
&= \iiint (u^P(\mathbf{x}, t, \mathbf{v}, X))^2 \, d\mathbf{x} \, d\mathbf{v} \, d\mathcal{P}_X.
\end{aligned} \tag{15}$$

Integrating (12) with respect to $\mathbf{x} \in \mathcal{D}_{per}$ and $\mathbf{v} \in \mathcal{V}_b$ leads to

$$\begin{aligned}
&\frac{d}{dt} \|u^P(t)\|_{L^2(\mathcal{I} \times \Theta)}^2 \\
&\leq 2\Sigma_t \iiint \sum_{k=0}^P u_k^2 + 2\Sigma_s \sum_{0 \leq k, q \leq P} \iiint (u_k(\mathbf{x}, t, \mathbf{v}') \phi_k u_q(\mathbf{x}, t, \mathbf{v}) \phi_q) \, d\mathcal{P}_X \, d\mathbf{v}' \, d\mathbf{v} \, d\mathbf{x}, \\
&\leq 2\Sigma_t \|u^P(t)\|_{L^2(\mathcal{I} \times \Theta)}^2 \\
&\quad + 2\Sigma_s \sum_{0 \leq k, q \leq P} \int \left[\int \left(\int u_k(\mathbf{x}, t, \mathbf{v}') \, d\mathbf{v}' \int u_q(\mathbf{x}, t, \mathbf{v}) \, d\mathbf{v} \right) d\mathbf{x} \right] \phi_k \phi_q \, d\mathcal{P}_X, \\
&\leq 2\Sigma_t \|u^P(t)\|_{L^2(\mathcal{I} \times \Theta)}^2 + 2\Sigma_s \sum_{k=0}^P \int \left(\int u_k(\mathbf{x}, t, \mathbf{v}) \, d\mathbf{v} \right)^2 \, d\mathbf{x}.
\end{aligned} \tag{16}$$

Finally, Jensen's inequality ensures we have

$$\partial_t \|u^P(t)\|_{L^2(\mathcal{I} \times \Theta)}^2 \leq 2(\Sigma_t + \Sigma_s) \|u^P(t)\|_{L^2(\mathcal{I} \times \Theta)}^2 \tag{17}$$

Gronwall's theorem allows obtaining the *a priori* bound

$$\|u^P(t)\|_{L^2(\mathcal{I} \times \Theta)} \leq e^{2(\Sigma_t + \Sigma_s)t} \|u_0^P\|_{L^2(\mathcal{I} \times \Theta)}. \tag{18}$$

It is therefore natural to seek solutions of the uncertain linear Boltzmann equation in the space $L^\infty([0, T] : L^2(\mathcal{I} \times \Theta))$. Here is the main result of this paper.

Theorem 1 (Convergence of the P -truncated gPC reduced model approximation) *Spectral accuracy holds in the following sense: for all $k \in \mathbb{N}$ with $k > 0$ such that $u \in H^k(\Theta)$, there exists a constant D_k such that $\forall t \in [0, T]$*

$$\|u(t) - u^P(t)\|_{L^2(\mathcal{I} \times \Theta)}^2 \leq e^{2(\Sigma_t + \Sigma_s)t} \left(\|u_0 - u_0^P\|_{L^2(\mathcal{I} \times \Theta)}^2 + 2(\Sigma_s + \Sigma_t)t \|u_0^2\|_{L^2(\mathcal{I} \times \Theta)} \frac{D_k}{p_{1D}^k} \right), \tag{19}$$

in which we recall P and p_{1D} are related via $P = P(p_{1D}, Q) = (p_{1D} + 1)^Q$.

Before proving the above result, we would like to comment on it. First, for different p_i per direction, spectral convergence only holds with respect to the coarser polynomial approximation amongst the directions $\{1, \dots, Q\}$ (this will be illustrated in section 4.3.1). Besides, with hypothesis 1, we have $\Sigma_s + \Sigma_t \geq 0$. As a consequence, the term $e^{2(\Sigma_t + \Sigma_s)t}$ may be a fast increasing factor. So, first, the term depending on the error on the initial condition, i.e. $e^{2(\Sigma_t + \Sigma_s)t} \|u_0 - u_0^P\|_{L^2(\mathcal{I} \times \Theta)}^2$, shows that any small error on the initial condition can be exponentially amplified. In other words, care must be taken to make sure the P -truncated approximation of the initial condition is accurate. The gPC framework [60, 66, 19], in opposition to the PC one [63, 10, 26], has been introduced precisely to this purpose: the initial polynomial basis must at least be able to fit accurately to the initial

uncertain condition to ensure a converging behaviour and avoid stagnation⁴. Second, the remaining term, i.e. $2(\Sigma_s + \Sigma_t)te^{2(\Sigma_t + \Sigma_s)t} \|u_0^2\|_{L^2(\mathcal{I} \times \Theta)} \frac{D_k}{p_{\text{ID}}^k}$, shows that even if care has been taken to make sure $\|u_0 - u_0^P\|_{L^2(\mathcal{I} \times \Theta)}^2 = 0$, the error can still grow quickly with time. It can be *theoretically* compensated with an increasing polynomial order P . The smoother the solution, the more efficient the increase of P . The fact the gPC reduced models present some difficulties with *long-term integration* is also well-known in the literature [61, 22]: it is here theoretically recovered (it will also be numerically recovered in section 4.1). Of course, in practice, increasing P is not straightforward as the reduced models will be harder and harder to solve as P grows. Still, in practice, with the following numerical example, we will show that the above bounds, even if enough to prove the fast convergence of the gPC reduced models for the uncertain linear Boltzmann equation, may be pessimistic and non-optimal. But before tackling numerical example, let us prove theorem 1.

Proof Assume u is a continuous solution of (4) and $u^P = \sum_{k=0}^P u_k \phi_k$ of the form (6) whose coefficients $(u_q)_{q \in \{0, \dots, P\}}$ solve (8). Then we suggest building an estimate of (we drop the dependencies for conciseness)

$$\partial_t \int_{\Theta} \frac{(u^P - u)^2}{2} d\mathcal{P}_X = \int_{\Theta} \left(\partial_t \frac{(u^P)^2}{2} - u^P \partial_t u - u \partial_t u^P + \partial_t \frac{u^2}{2} \right) d\mathcal{P}_X.$$

Unknowns u and $(u_0, \dots, u_P)^t$ being strong solutions of (4) and (8), we have

$$\begin{aligned} \partial_t \int_{\Theta} \frac{(u^P - u)^2}{2} &= - \int_{\Theta} \mathbf{v} \cdot \nabla_{\mathbf{x}} \frac{u^2}{2} - \int_{\Theta} v \sigma_t u^2 + v \int_{\Theta} \sigma_s u \int u \\ &\quad + \int_{\Theta} u^P \mathbf{v} \cdot \nabla_{\mathbf{x}} u + v \int_{\Theta} \sigma_t u^P u - v \int_{\Theta} \sigma_s u^P \int u \\ &\quad + \int_{\Theta} u \mathbf{v} \cdot \nabla_{\mathbf{x}} u^P + v \int_{\Theta} \sigma_t u^P u - v \int_{\Theta} \sigma_s u \int u^P \\ &\quad - \int_{\Theta} \mathbf{v} \cdot \nabla_{\mathbf{x}} \frac{(u^P)^2}{2} - v \int_{\Theta} \sigma_t (u^P)^2 + v \int_{\Theta} \sigma_s u^P \int u^P. \end{aligned}$$

Integration with respect to $\mathbf{x} \in \mathcal{D}_{\text{per}}$, $\mathbf{v} \in \mathcal{V}_b$ yields

$$\begin{aligned} \frac{d}{dt} \iiint_{\Theta} \frac{(u^P - u)^2}{2} &= - \iiint_{\Theta} \mathbf{v} \cdot \nabla_{\mathbf{x}} \frac{u^2}{2} - \iiint_{\Theta} v \sigma_t u^2 + v \iiint_{\Theta} \sigma_s u \int u \\ &\quad + \iiint_{\Theta} u^P \mathbf{v} \cdot \nabla_{\mathbf{x}} u + \iiint_{\Theta} v \sigma_t u^P u - v \iiint_{\Theta} \sigma_s u^P \int u \\ &\quad + \iiint_{\Theta} u \mathbf{v} \cdot \nabla_{\mathbf{x}} u^P + \iiint_{\Theta} v \sigma_t u^P u - v \iiint_{\Theta} \sigma_s u \int u^P \\ &\quad - \iiint_{\Theta} \mathbf{v} \cdot \nabla_{\mathbf{x}} \frac{(u^P)^2}{2} - \iiint_{\Theta} v \sigma_t (u^P)^2 + v \iiint_{\Theta} \sigma_s u^P \int u^P. \end{aligned}$$

The terms in the above expression cancel due to the hypothesis of having periodic boundary conditions. For the same reason we have $\int_{\mathcal{D}_{\text{per}}} u^P \nabla_{\mathbf{x}} u d\mathbf{x} = \int_{\partial \mathcal{D}_{\text{per}}} (u^P u) \cdot \mathbf{n} d\sigma - \int_{\mathcal{D}_{\text{per}}} u \nabla_{\mathbf{x}} u^P d\mathbf{x}$ so that the previous expression becomes

$$\begin{aligned} \frac{d}{dt} \iiint_{\Theta} \frac{(u^P - u)^2}{2} &= - \iiint_{\Theta} v \sigma_t u^2 + \iiint_{\Theta} v \sigma_s u \int u \\ &\quad + \iiint_{\Theta} v \sigma_t u^P u - \iiint_{\Theta} v \sigma_s u^P \int u \\ &\quad + \iiint_{\Theta} v \sigma_t u^P u - \iiint_{\Theta} v \sigma_s u \int u^P \\ &\quad - \iiint_{\Theta} v \sigma_t (u^P)^2 + \iiint_{\Theta} v \sigma_s u^P \int u^P. \end{aligned}$$

⁴Indeed, if $\|u_0 - u_0^P\|_{L^2(\mathcal{I} \times \Theta)}^2 = C_0 \neq 0$, then $\|u(t) - u^P(t)\|_{L^2(\mathcal{I} \times \Theta)}^2 \xrightarrow{P \rightarrow \infty} C_0 e^{2(\Sigma_s + \Sigma_t)t}$ for fixed time t .

Let us now define $\pi_P u$ the orthogonal projector of u solution to (4) in $L^2(\Theta)$ onto the space $(\phi_k)_{k \in \{0, \dots, P\}}$. The previous expression can be equivalently rewritten

$$\begin{aligned} \frac{d}{dt} \iiint_{\Theta} \frac{(u^P - u)^2}{2} &= - \iiint_{\Theta} v \sigma_t u^2 && + \iiint_{\Theta} v \sigma_s u \int u \\ &+ \iiint_{\Theta} v \sigma_t u^P \pi_P u && - \iiint_{\Theta} v \sigma_s u^P \int \pi_P u \\ &+ \iiint_{\Theta} v \sigma_t u^P \pi_P u && - \iiint_{\Theta} v \sigma_s \pi_P u \int u^P \\ &- \iiint_{\Theta} v \sigma_t (u^P)^2 && + \iiint_{\Theta} v \sigma_s u^P \int u^P. \end{aligned}$$

Let us now rearrange the terms as

$$\begin{aligned} \frac{d}{dt} \iiint_{\Theta} \frac{(u^P - u)^2}{2} &= \\ &+ \iiint_{\Theta} v \sigma_t (2u^P (\pi_P u - u) - (u^P - u)^2) && + \iiint_{\Theta} v \sigma_s \left((u - u^P) \left[\int u - \int u^P \right] \right) \\ &&& + \iiint_{\Theta} v \sigma_s \left(-u^P \int (\pi_P u - u) - (\pi_P u - u) \int u^P \right). \end{aligned}$$

From hypothesis (1), we obtain

$$\begin{aligned} \frac{d}{dt} \iiint_{\Theta} \frac{(u^P - u)^2}{2} &\leq +2\Sigma_t \left| \iiint_{\Theta} u^P (\pi_P u - u) \right| && + \Sigma_s \iint_{\Theta} \left(\int (u - u^P) \right)^2 \\ &+ \Sigma_t \iiint_{\Theta} (u^P - u)^2 && + 2\Sigma_s \left| \iint_{\Theta} \left(\int u^P \int (\pi_P u - u) \right) \right|. \end{aligned}$$

From Jensen's inequality, we have

$$\begin{aligned} \frac{d}{dt} \iiint_{\Theta} \frac{(u^P - u)^2}{2} &\leq +2(\Sigma_t + \Sigma_s) \iiint_{\Theta} \frac{(u - u^P)^2}{2} && + 2\Sigma_t \left| \iiint_{\Theta} u^P (\pi_P u - u) \right| \\ &&& + 2\Sigma_s \left| \iint_{\Theta} \left(\int u^P \int (\pi_P u - u) \right) \right|, \end{aligned}$$

to finally get (Hölder inequality)

$$\begin{aligned} \frac{d}{dt} \|(u - u^P)(t)\|_{L^2(\mathcal{I} \times \Theta)}^2 &\leq +2(\Sigma_t + \Sigma_s) \|(u - u^P)(t)\|_{L^2(\mathcal{I} \times \Theta)}^2 \\ &+ 2(\Sigma_t + \Sigma_s) \|u^P(t)\|_{L^2(\mathcal{I} \times \Theta)} \times \|(\pi_P u - u)(t)\|_{L^\infty(\mathcal{I} \times \Theta)}. \end{aligned}$$

Let us now work on the last term of the previous expression. Thanks to (18), we are able to bound

$$\begin{aligned} \frac{d}{dt} \|(u - u^P)(t)\|_{L^2(\mathcal{I} \times \Theta)}^2 &\leq +2(\Sigma_t + \Sigma_s) \|(u - u^P)(t)\|_{L^2(\mathcal{I} \times \Theta)}^2 \\ &+ 2(\Sigma_t + \Sigma_s) e^{2(\Sigma_s + \Sigma_t)t} \|u_0^P\|_{L^2(\mathcal{I} \times \Theta)} \times \|\pi_P u - u\|_{L^\infty(\mathcal{I} \times \Theta)}. \end{aligned} \quad (20)$$

This means it only remains to be able to deal with the L^∞ -norm of $\pi_P u - u$ to conclude.

In the following for simplicity of notations, without loss of generality, we carry out the calculations with $X \in \mathbb{R}^{Q=1}$. Now, the truncation of the expansion gives

$$u(\mathbf{x}, t, \mathbf{v}, X) - \pi_{p_{1D}} u(\mathbf{x}, t, \mathbf{v}, X) = \sum_{n=p_{1D}+1}^{\infty} \phi_n(X) \int u(\mathbf{x}, t, \mathbf{v}, X) \phi_n(X) d\mathcal{P}_X,$$

Furthermore, orthonormal polynomials $(\phi_k)_{k \in \{0, \dots, p_{1D}\}}$ are known to be the eigenvectors of the eigenproblem (see [2])

$$\left(Q(\xi) \frac{d^2}{d\xi^2} + L(\xi) \frac{d}{d\xi} \right) \phi(\xi) = \lambda \phi(\xi), \quad (21)$$

where Q and L are respectively second and first order polynomials and $\lambda_k = -k(\frac{k-1}{2}Q'' + L')$, $\forall k \in \mathbb{N}$. For example, for Legendre polynomials, $Q(\xi) = 1 - \xi^2$, $L(\xi) = -2\xi$ and the eigenvalues are $k(k+1)$, $\forall k \in \mathbb{N}$. For Hermite polynomials (related to the gaussian distribution), $Q(\xi) = 1$, $L(\xi) = -2\xi$ and $\lambda_k = 2k$, $\forall k \in \mathbb{N}$. As a consequence, we have

$$\left(Q(\xi) \frac{d^2}{d\xi^2} + L(\xi) \frac{d}{d\xi} \right) [u(\mathbf{x}, t, \mathbf{v}, \xi) - \pi_{p_{1D}} u(\mathbf{x}, t, \mathbf{v}, \xi)] = \sum_{k=p_{1D}+1}^{\infty} \lambda_k \phi_k(\xi) \int u(\mathbf{x}, t, \mathbf{v}, X) \phi_k(X) d\mathcal{P}_X.$$

Since the derivative of u with respect to ξ are bounded in L^2_{Θ} up to order k by hypothesis (9), we have

$$\sum_{j=p_{1D}+1}^{\infty} \left[\int u(\mathbf{x}, t, \mathbf{v}, X) \phi_j(X) d\mathcal{P}_X \right]^2 \lambda_j^{2m} < \infty, \quad \forall m \in \{0, \dots, \lfloor \frac{k}{2} \rfloor\}, \quad \forall t \in [0, T], (\mathbf{x}, \mathbf{v}) \in \mathcal{I}. \quad (22)$$

Finally, one has the bound for all $t \in [0, T]$, $(\mathbf{x}, \mathbf{v}) \in \mathcal{I}$ and $\forall m \in \{0, \dots, \lfloor \frac{k}{2} \rfloor\}$

$$\begin{aligned} & \|u(\mathbf{x}, t, \mathbf{v}, \cdot) - \pi_{p_{1D}} u(\mathbf{x}, t, \mathbf{v}, \cdot)\|_{L^\infty(\Theta)} \\ & \leq \sum_{n=p_{1D}+1}^{\infty} \left| \int u(\mathbf{x}, t, \mathbf{v}, X) \phi_n(X) d\mathcal{P}_X \right| \|\phi_n\|_{L^\infty(\Theta)} \\ & \leq \left(\sum_{n=p_{1D}+1}^{\infty} \left[\int u(\mathbf{x}, t, \mathbf{v}, X) \phi_n(X) d\mathcal{P}_X \right]^2 \lambda_n^{2m} \right)^{\frac{1}{2}} \left(\sum_{n=p_{1D}+1}^{\infty} \frac{\|\phi_n\|_{L^\infty(\Theta)}^2}{\lambda_n^{2m}} \right)^{\frac{1}{2}}. \end{aligned} \quad (23)$$

The first sum is bounded, cf. (22). The second term deserves some more attention.

Hypothesis 2 *Without loss of generality (see (3) and the relative discussion), we can always consider that, up to change of variable (3), X is uniformly distributed and $(\phi_k^L)_{k \in \mathbb{N}}$ are the Legendre polynomials.*

Under the previous condition, we have the bound [2] $\forall n \in \mathbb{N}$

$$\|\phi_n^L\|_{L^\infty(\Theta)} \leq C(n+1)^{\frac{1}{2}}. \quad (24)$$

Remark 3.2 *Note that in the above lines, care has been taken to have resort to hypothesis 2 the later possible. In practice, avoiding this change of variable is complex, especially if X is an unbounded random variable. In other words, we intensively used the fact that any unbounded random variable X (such that hypothesis 1 and condition (9) are fulfilled) can be mapped into an uniform one \mathcal{U} . The theorem supposes performing, even in the gaussian case for X for example, a gPC development on the Legendre basis with respect to $\mathcal{U} = F_G^{-1}(X)$ where $X \rightarrow F_G(X)$ is the cumulative density function of the gaussian distribution. Theorem 1 does not really predict the behaviour of a Hermite-gPC based reduced model with X gaussian (even if they are known to perform well for many applications, see [26]). To be able to conclude for an arbitrary random variable X ⁵, we would both need to show that $\|\phi_n^X\|_{L^\infty(\Theta)}$ is bounded and, more than bounded, grows with n less quickly than λ_n^k . In [40], the authors study conditions on $d\mathcal{P}_X$ to obtain bounds of $\|\phi_n^X(\xi) \frac{d\mathcal{P}_X}{d\xi}(\xi)\|_{L^\infty(\Theta)}$ defined on an unbounded space. Note that those bounds does not grow too fast with n , see [40]. In other words, the equivalent of (24) for arbitrary weighted polynomials $(\phi_k^X \frac{d\mathcal{P}_X}{d\xi})_{k \in \mathbb{N}}$ may be at hand. But the crucial step remains to be able to go from (23) to an inequality involving $\|\phi_n^X(\xi) \frac{d\mathcal{P}_X}{d\xi}(\xi)\|_{L^\infty(\Theta)}$. To our knowledge, this point is not straightforward but would stand for the last step to conclude of the spectral convergence of the gPC based reduced models without having resort to hypothesis 2. Avoiding it may lead to finer bounds for an arbitrary random vector X .*

⁵together with its associated polynomial basis $(\phi_k^X)_{k \in \mathbb{N}}$, orthonormal with respect to the scalar product defined by $d\mathcal{P}_X$.

As a consequence, with the above (uniform/Legendre) hypothesis and (24), there exists a constant C_k such that

$$\|u(\mathbf{x}, t, \mathbf{v}, \cdot) - \pi_P u(\mathbf{x}, t, \mathbf{v}, \cdot)\|_{L^\infty(\Theta)} \leq \frac{C_k}{P_{1D}^k} \quad (25)$$

Finally, putting together (20)–(25) and invoking Gronwall’s theorem allows ending the proof of theorem 1. \blacksquare

In the following section, we present some numerical results. Most of them confirm the result of theorem 1. Some of them aim at going beyond it and tackle perspectives and open problems.

4 Numerical application

In this last section, we present some numerical results obtained from the resolution of P –truncated gPC reduced models. In sections 4.1 and 4.3, we consider simple (1D physical, 1D stochastic or 2D physical, 3D stochastic) configurations for which analytical solutions are available. With the construction of analytical solutions (sections 4.1 and 4.3), we aim at showing we can numerically recover the results of theorem 1 (spectral convergence, long-term behaviour, independently of the considered dimension). Due to this constraint⁶, the test-cases may appear physically simple. The reader interested in more complex test-problems with some high dimensional resolutions of (4) can refer to [50].

In section 4.2, we consider a (2D physical, 1D stochastic) test-case for which, to our knowledge, no analytical solution is available. It shows that complex (non-analytical) configurations can be handled and that the fast convergence rate of the gPC reduced models can still be numerically observed.

Finally, in the next sections, several numerical methods are used: analytical ODE resolution and explicit Euler scheme in sections 4.1 and 4.3, an MC scheme [50] in sections 4.2 and 4.3.1, an S_n -like resolution (see [4, 16, 12]) in section 4.3.2. The diversity of numerical schemes aims at showing that the results of theorem 1 are independent of the resolution methods for system (10).

4.1 A first simple homogeneous uncertain configuration

In this first numerical section, we compare the results obtained from P –truncated gPC reduced models to an analytical solution. We aim at numerically recovering the fast convergence rate demonstrated in theorem 1. The test-problem has already been introduced in [50] but we tackle it from a different point of view (convergence with respect to P here).

Let us consider a monokinetic (i.e. $v = 1$) homogeneous (i.e. $u(\mathbf{x}, t, \mathbf{v}, X) = u(t, \omega, X)$) configuration. We assume the uncertainty, one-dimensional here for the sake of simplicity, affects the scattering cross-sections $\sigma_s = \bar{\sigma}_s + \hat{\sigma}_s X$, where $X \sim \mathcal{U}[-1, 1]$. Of course, $\hat{\sigma}_s$ is closely related to the variance of the uncertain scattering cross-section. Let us introduce $U(t, X) = \int u(t, \omega, X) d\omega$. In the previously described configuration, the uncertain linear Boltzmann equation resumes to the following stochastic ordinary differential equation (ODE)

$$\begin{cases} \partial_t U(t, X) + v\sigma_t U(t, X) = v\sigma_s(X)U(t, X), \\ U(0) = U_0. \end{cases} \quad (26)$$

Introduce $\sigma_a = \sigma_t - \sigma_s$, then the solution is given by

$$U(t, X) = U_0 e^{-v\sigma_a(X)t} = U_0 e^{-v(\sigma_t - \bar{\sigma}_s - \hat{\sigma}_s X)t} = U_0 e^{-v(\bar{\sigma}_a - \hat{\sigma}_s X)t}. \quad (27)$$

⁶i.e. being able to build an analytical solution.

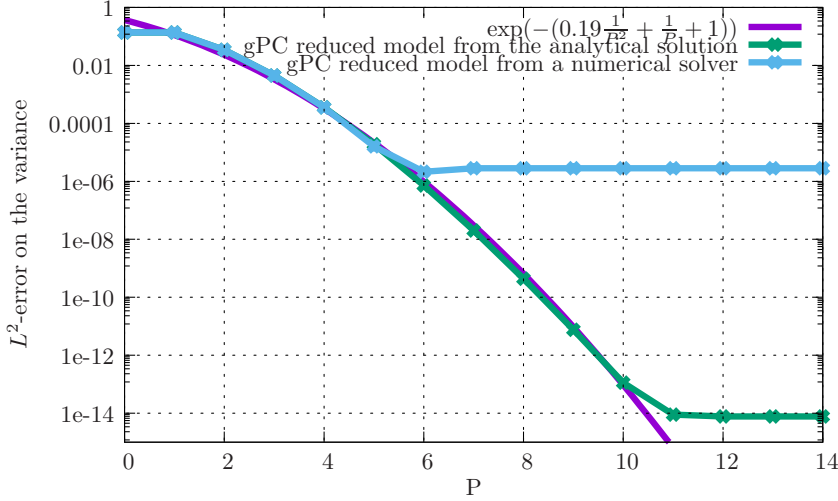


Figure 1: Convergence study with respect to P obtained with numerically computed solution of the gPC reduced model. The plot also displays the function $P \rightarrow \exp(-0.19\frac{1}{P^2} + \frac{1}{P} + 1)$.

The quantity $U(t, X)$ is a random variable indexed by time t , i.e. it is a stochastic process. In this case, mean and variance of the stochastic process (27) can be computed analytically and are given by

$$\begin{aligned}
M_1^U(t) = \mathbb{E}[U(t, X)] &= \frac{1}{2}U_0 e^{-v\bar{\sigma}_a t} \frac{e^{v\hat{\sigma}_s t} - e^{-v\hat{\sigma}_s t}}{\hat{\sigma}_s t v}, \\
M_2^U(t) = \mathbb{E}[U^2(t, X)] &= \frac{1}{4}U_0^2 e^{-2v\bar{\sigma}_a t} \frac{e^{2v\hat{\sigma}_s t} - e^{-2v\hat{\sigma}_s t}}{\hat{\sigma}_s t v}, \\
\mathbb{V}[U](t) &= M_2^U(t) - (M_1^U(t))^2.
\end{aligned} \tag{28}$$

Of course, higher order moments, probability of failure, complete characterisation of the probability density function of the stochastic process can be calculated but in figure 1 we focus on the variance $\mathbb{V}[U](t)$ to perform the convergence studies.

Our aim now is to compare the results obtained from a P -truncated gPC based reduced model and the analytical ones. In this particular configuration, the reduced model (10) resumes to a system of coupled ODEs

$$\partial_t \begin{pmatrix} U_0(t) \\ \dots \\ U_P(t) \end{pmatrix} = \Sigma_a \begin{pmatrix} U_0(t) \\ \dots \\ U_P(t) \end{pmatrix}, \tag{29}$$

with

$$\Sigma_a = \begin{pmatrix} \sum_{k=0}^P \int \sigma_a \phi_0 \phi_0 d\mathcal{P}_X & \dots & \sum_{k=0}^P \int \sigma_a \phi_0 \phi_P d\mathcal{P}_X \\ \dots & \sum_{k=0}^P \int \sigma_a \phi_i \phi_j d\mathcal{P}_X & \dots \\ \sum_{k=0}^P \int \sigma_a \phi_P \phi_0 d\mathcal{P}_X & \dots & \sum_{k=0}^P \int \sigma_a \phi_P \phi_P d\mathcal{P}_X \end{pmatrix}.$$

The solution of the above system is the exponential of matrix Σ_a with initial condition $(U_0^0, \dots, U_P^0)^t$. It can be computed analytically with any algebraic computation software for arbitrary order P . Note that we also verified that the use of fine non intrusive resolution (with Gauss-Legendre points) gives

equivalent results. The results presented in figure 1 compare the variance obtained from the analytical solution (28) and the variance obtained from the analytical solution of (29). Figure 1 displays three curves:

- the first one corresponds to a convergence study with respect to P of the L^2 -norm of the error of U solution of (26) and $U^P = \sum_{k=0}^P U_k \phi_k$ where $(U_0, \dots, U_P)^t$ is solution of (29).
- The second one corresponds to a plot of function $P \rightarrow \exp(-0.19 \frac{1}{P^2} + \frac{1}{P} + 1)$.
- The last curve corresponds to the same convergence study except $(U_0, \dots, U_P)^t$, solution of (29), is obtained numerically. We use an explicit Euler scheme of time step $\Delta t = 10^{-7}$.

Note that in practice, we take $v = 1, U_0 = 1, \sigma_t = 1, \bar{\sigma}_s = 0.8, \hat{\sigma}_s = 0.3$. The first curve, the convergence study comparing the analytical solutions of (26) and (29), testifies of a fast converging behaviour of U^P toward U as P increases. Machine accuracy is reached as soon as $P = 10$. The curve $P \rightarrow \exp(-0.19 \frac{1}{P^2} + \frac{1}{P} + 1)$ perfectly fits the latter, up to order $P = 10$. It means the convergence rate observed here is even faster than the one predicted by theorem 1. Of course, theorem 1 has been proved in more general conditions. But the latter numerical result also probably shows the bounds of theorem 1 are not optimal, at least for homogeneous problems. The convergence study obtained from a numerically solved system (29) (figure 1 right) presents the same behaviour as the analytical convergence curve up to order $P = 6$: for higher truncation order, the solution is $\mathcal{O}(\Delta t) \approx 10^{-6}$ and P is not anymore the constraining parameter.

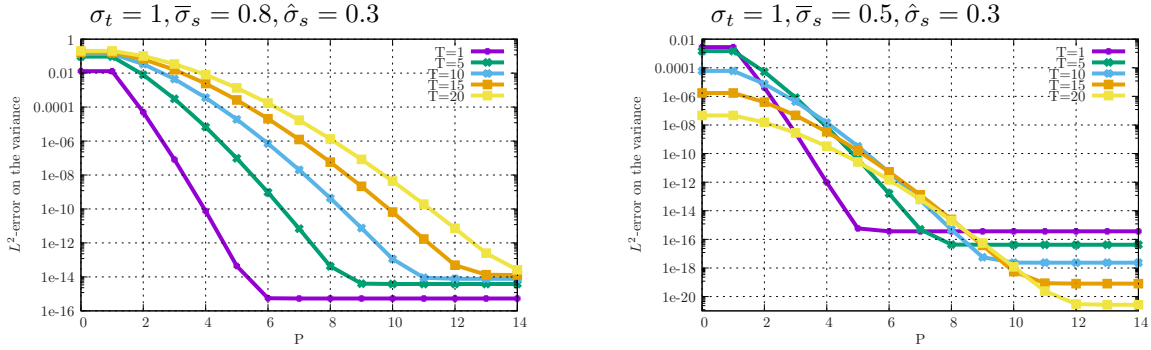


Figure 2: Left: convergence study with respect to P obtained with an analytical gPC reduced model and a numerically obtained one for parameters $\sigma_t = 1, \bar{\sigma}_s = 0.8, \hat{\sigma}_s = 0.3$ for several final times $T = 1, 5, 10, 20$. Right convergence study with respect to P obtained with an analytical gPC reduced model and a numerically obtained one for parameters $\sigma_t = 1, \bar{\sigma}_s = 0.5, \hat{\sigma}_s = 0.3$ for several final times $T = 1, 5, 10, 20$.

Figure 2 presents the same kind of convergence studies for different final times $T = 1, 5, 10, 20$ and for different values of $\bar{\sigma}_s$ controlling the variability of the uncertainty in the scattering cross-section. ($\bar{\sigma}_s = 0.8$ for the left picture, $\bar{\sigma}_s = 0.5$ for the right one). Let us begin with figure 2 (left). It corresponds to the case $\sigma_t = 1, \bar{\sigma}_s = 0.8, \hat{\sigma}_s = 0.3$: for these values of cross-sections, there exists some realizations X such that $\bar{\sigma}_s + \hat{\sigma}_s X > \sigma_t$ with $\mathbb{P}(\bar{\sigma}_s + \hat{\sigma}_s X > \sigma_t) > 0$. In other words, the medium can be multiplicative with a non-negligible probability. Figure 2 (left) presents the convergence studies obtained with the previous parameters for different final times T . Once again, we recover the behaviour predicted by theorem 1: first, spectral convergence is ensured independently of the final time T . Second, the later the final time T , the higher the error on the variance. Indeed, as $\forall P \in \{0, \dots, 14\}$, the error for early times is lower than the error for later times: this puts forward the fact that the long-term behaviour (i.e. fast increase of the error with time) hinted at in the comments on theorem 1 in section 3 can occur in practice. Still, acceptable error remains reachable as, for example, $P = 10$ still ensures an

accuracy below 10^{-8} (which is two digits below the numerical error $\mathcal{O}(\Delta t) = 10^{-6}$ for example). Figure 2 (right) presents the same convergence studies but with $\sigma_t = 1, \bar{\sigma}_s = 0.5, \hat{\sigma}_s = 0.3$: for these values of cross-sections, the set $\{X \in [-1, 1] | \bar{\sigma}_s + \hat{\sigma}_s X > \sigma_t\}$ is such that $\mathbb{P}(\bar{\sigma}_s + \hat{\sigma}_s X > \sigma_t) = 0$. In other words, the medium can never be multiplicative, it is absorbing with probability 1. The convergence studies of figure 2 (right) tend to put forward the fact the coefficient in the exponential in (19) is negative whereas this possibility is not predicted by theorem 1. As a consequence, the error, in this case, decreases with time: for example, an accuracy of 10^{-8} is reached as soon as $P = 4$ for $T \leq 20$. In this simple uncertain configuration, the reduced models behave even better than predicted by (19) in theorem 1: in other words, this test-case puts forward the fact that the bounds in theorem 1 are certainly not optimal in *absorbing* media.

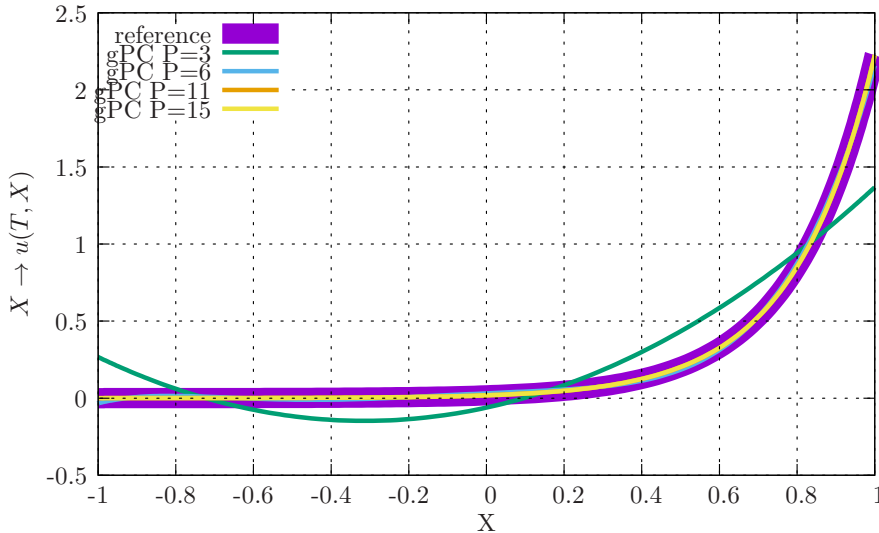


Figure 3: Reference solution $X \rightarrow U(T, X) = U_0 e^{-v(\sigma_t - \bar{\sigma}_s - \hat{\sigma}_s X)T}$ for final time $T = 20$ together with four gPC approximations for $P = 3, 6, 11, 15$.

Figure 3 presents another kind of convergence study. It displays the reference solution $X \rightarrow U(X, T)$ for final time $T = 20$ together with four gPC approximations $X \rightarrow U^P(T, X) = \sum_{k=0}^P U_k(T) \phi_k(X)$ obtained for $P = 3, 6, 11, 15$. Once again, the fast convergence is observed as only the coarser gPC approximation ($P = 3$) is discernable from the analytical solution. Above all, this study puts forward the fact that the gPC approximations *do not necessarily preserve the positivity of the solution* $X \rightarrow U(T, X)$: indeed, for $P = 3$, the gPC approximation goes under zero predicting a non-zero probability of having a negative density of particles. But thanks to the fast converging behaviour of U^P with respect to P , positivity is recovered for higher orders (for this test-problem, as soon as $P = 9$). Of course, nothing ensures that $P = 9$ will be enough for later times $t > T$ (cf. the remark on the long-term behaviour of gPC tackled in the previous paragraphs). It is difficult having an *a priori* idea of the necessary order to preserve positiveness but in practice, accurate results remain available for relatively small polynomial orders P on relevant statistical quantities (see [50] for complementary studies). Note that several interesting methods have been introduced in order to preserve certain properties of the system of interest (hyperbolicity, positiveness, maximum principle see [15, 54, 18, 32]) and may be combined to the material of this paper.

In the next section, we consider a test-case for which, to our knowledge, no analytical solution is available. We will have resort to the numerical scheme described in [50].

4.2 Taking into account uncertainties in the scattering cross-section

Let us now tackle a new test-problem for which an analytical solution is not available despite the relative simplicity of the configuration. Note that care has been taken to consider a configuration different from the ones of [50]. We aim at making this paper and [50] complementary.

Let us present the detail of the next study:

- let us consider $\mathbf{x} = x \in \mathcal{D} = [0, 1]$.
- We assume the particles are monokinetic with $v = 1$.
- Besides, we assume that the medium is only diffusive (no absorption, i.e. $\sigma_t = \sigma_s$) and the cross-sections are deterministic. We choose $\sigma_s = \sigma_t = 1$.
- We here want to take into account uncertainties in the distribution of the scattering angle P , see expression (13). Let us consider a monodimensional uncertain parameter (i.e. $Q = 1$) and assume it is uniformly distributed in $[-1, 1]$, i.e. $X \sim \mathcal{U}([-1, 1])$. The uncertain parameter X affects the outer angular distribution. With the above hypothesis (monodimensional and monokinetic) we have $P_s(x, t, \mathbf{v}, \mathbf{v}', X) = P_s(\omega', X)$. Furthermore in this test-problem, we assume P_s is not isotropic and uncertain. We assume we have

$$P_s(\omega', X) d\omega' = \mathbf{1}_{[0, U(X)]}(\omega'),$$

where $X \rightarrow U(X) = 0.8 \frac{(X+1)}{2}$ maps X in $[-1, 1]$ into a uniformly distributed random variable $U(X)$ in $[0, 0.8]$. As a consequence, the scattering is always anisotropic and depending on the realizations of X , the scattering angle can be sampled in a narrower band than $[0, 0.8]$. Note that $\omega' \rightarrow P_s(\omega', X)$ is positive and sums up to 1, $\forall X \in [-1, 1]$: it is always a probability density function and the scattering angle always has sense. The expression of the scattering angle distribution may appear singular for the reader familiar with the linear Boltzmann equation (neutronics or photonics for example). At this stage of the discussion, we can already explain it has been chosen simple (for ease of reproduction of the numerical results)..

- The initial condition is a Heaviside between 0 and $\frac{1}{50}$, i.e. we have a deterministic initial condition given by $u_0(x, \omega) = \mathbf{1}_{[0, \frac{1}{50}]}(x)$.

In this particular case, (4) resumes to

$$\begin{cases} \partial_t u(x, t, \omega, X) + v\omega \partial_x u(x, t, \omega, X) = -v\sigma_s u(x, t, \omega, X) + v\sigma_s \int P_s(\omega', X) u(x, t, \omega', X) d\omega', \\ u(x, 0, \omega) = u_0(x) = \mathbf{1}_{[0, \frac{1}{50}]}(x). \end{cases} \quad (30)$$

Note that in the next study, we take specular boundary condition on both sides of domain $\mathcal{D} = [0, 1]$. In other words, the particles hit walls with perfect reflection at $x = 0$ and $x = 1$. The computation has been made by the Monte-Carlo scheme described in [50]. It has $N_x = 50$ cells, but they are only used for visualisation. The most important numerical parameter for such a numerical solver is the number of MC particles $N_{MC} = 2.8 \times 10^7$ (see [50] for more details on the resolution scheme).

Figure 4 presents the numerical results obtained in this configuration. Let us introduce notation $U(x, t, X) = \int u(x, t, \omega, X) d\omega$. Let us furthermore introduce $\forall k \in \{0, \dots, P\}$

$$U_k(x, t) = \int u_k(x, t, \omega) d\omega = \iint u(x, t, \omega, X) \phi_k(X) d\mathcal{P}_X d\omega. \quad (31)$$

Then $U^P(x, t) = \sum_{k=0}^P U_k(x, t) \phi_k(X)$ is an approximation of $U(x, t)$ obtained from the numerical resolution of reduced model (8). Approximations of the mean and variance are easily obtained from

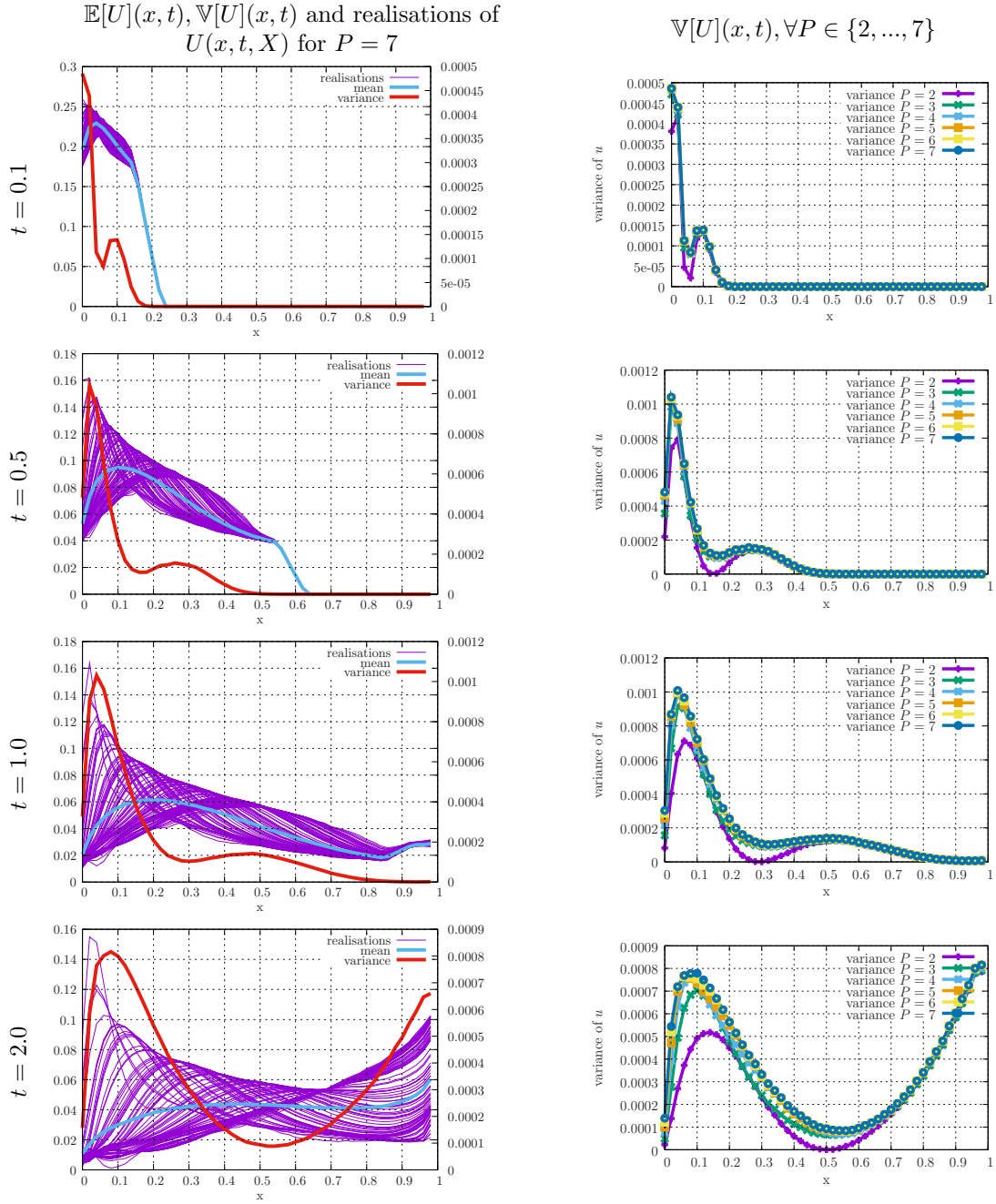


Figure 4: All the results of this figure have been obtained applying the gPC-i-MC scheme of [50]. Left: time evolution of the mean and variance profiles together with 200 realisations recovered thanks to the use of $P = 7$ -truncated gPC reduced model. Right: convergence studies on the variance of U with respect to P in the same condition as for the left column (time evolution of the profiles of the variance for $P \in \{2, \dots, 7\}$).

U^P as we have

$$\begin{aligned} \mathbb{E}[U](x, t) &\approx \mathbb{E}[U^P](x, t) = U_0(x, t), \\ \mathbb{V}[U](x, t) &\approx \mathbb{V}[U^P](x, t) = \sum_{k=1}^P U_k^2(x, t). \end{aligned} \quad (32)$$

Many other classical statistical quantities can be obtained from post-treatments of the gPC coefficients, see [6]. Some examples (Sobol indices) are given in [50].

Figure 4 (left) displays $\mathbb{E}[U^{P=7}](x, t)$, $\mathbb{V}[U^{P=7}](x, t)$ and N realizations of $U^{P=7}(x, t, X)$ for $N = 100$ uniformly distributed $(X_i)_{i \in \{1, \dots, N\}} \sim \mathcal{U}([-1, 1])$ for several times $t \in \{0.1, 0.5, 1.0, 2.0\}$. Note that on figure 4 (left), the left axis corresponds to the scale for the mean and the realizations whereas the right axis corresponds to the scale for the variance. Figure 4 (right) presents a convergence study with respect to P for the spatial profiles of the variance.

Let us first focus on figure 4 (left) and on a description of the test-case. The initial condition is deterministic and consists in a Heaviside of particles along the left wall. We begin by the description of the average behaviour, the mean $\mathbb{E}[U^{P=7}](x, t)$. At time $t = 0.1$ (figure 4 top left), particles are evolving in the random medium. The bulk is propagating toward the right hand side but some particles remain in the vicinity of the wall due to the scattering they encounter. As time passes, the average population of particles goes toward the right wall and are reflected toward the center of the domain. From a variance point of view, uncertainties are affecting the particles as soon as $t > 0$. The area of highest variance remains in the vicinity of the left boundary but grows as the flow of particles propagates to the right hand side of domain \mathcal{D} . This is all the more emphasized by the realisations of $U^P(x, t)$ on the same pictures: for the three earliest times $t = 0.1, 0.5, 1.0$, the front of the particle propagation has a zero variance. The positive variance is only in the wake of the particle flow. After the reshock on the right boundary, the whole domain is affected by a positive variance. The right column of figure 4 presents the variance of U^P for $P \in \{2, \dots, 7\}$ for the same times. Once again, for early times, the convergence is fast: $P \in \{3, \dots, 7\}$ gives almost the same results, only the solution obtained from the $P = 2$ -truncated reduced model presents a coarse behaviour at this time. As time increases, the differences between the several reduced model results become more and more visible. At time $t = 2.0$, the need for higher truncation orders P is visible. On this same picture, the fast convergence is noticeable, even without having access to an analytical solution, as the gaps between the solutions obtained with P and $P + 1$ are decreasing quickly with P .

4.3 Two multidimensional 5D (2D physical and 3D stochastic) test-case

In this section, we consider two multidimensional test-cases for which we can build analytical solutions. The configurations remain simple, despite the quite important number of dimensions and are probably not enough representative of physical applications (we refer to [50] for more relevant ones). But having access to analytical solutions allow verifying the results of theorem 1 are valid in higher dimensions.

4.3.1 A smooth 5D analytical problem

Let us begin by a smooth 5D (2D physical and 3D stochastic) problem and its description: we consider $\mathbf{x} = x \in \mathcal{D} = [0, 2]$. We assume the particles are monokinetic with $v = 1$. Besides, we assume that the scattering particles do not change directions: the medium can be absorbing or even multiplicative but we assume (13) is given by $P_s(\omega, \omega') d\omega' = \delta_{\omega'}(\omega)$. In other words, a particle encountering a scattering event, (absorbing or multiplicative) does not change its direction. The uncertainty, in 3D stochastic dimension, affects the cross-sections as

$$- \sigma_t(X) = \sigma_t(X_1, X_2) = (\bar{\sigma}_t + \hat{\sigma}_t X_2) (\bar{\eta} + \hat{\eta} X_1),$$

$$- \sigma_s(X) = \sigma_s(X_1, X_3) = (\bar{\sigma}_s + \hat{\sigma}_s X_3) (\bar{\eta} + \hat{\eta} X_1).$$

- In the expressions above, $\eta(X) = \bar{\eta} + \hat{\eta}(X_1)$ acts like an unknown density of matter for example.

- We assume $X = (X_1, X_2, X_3)^t$ is a vector of independent uniform random variables on $[-1, 1]$.

The initial condition is a Dirac at $x_0 = 1$, i.e. we have a deterministic initial condition given by $u_0(x, \omega) = \delta_{x_0}(x)$. The cross-sections and the initial condition are such that (respectively) condition (9) and hypothesis 1 are fulfilled.

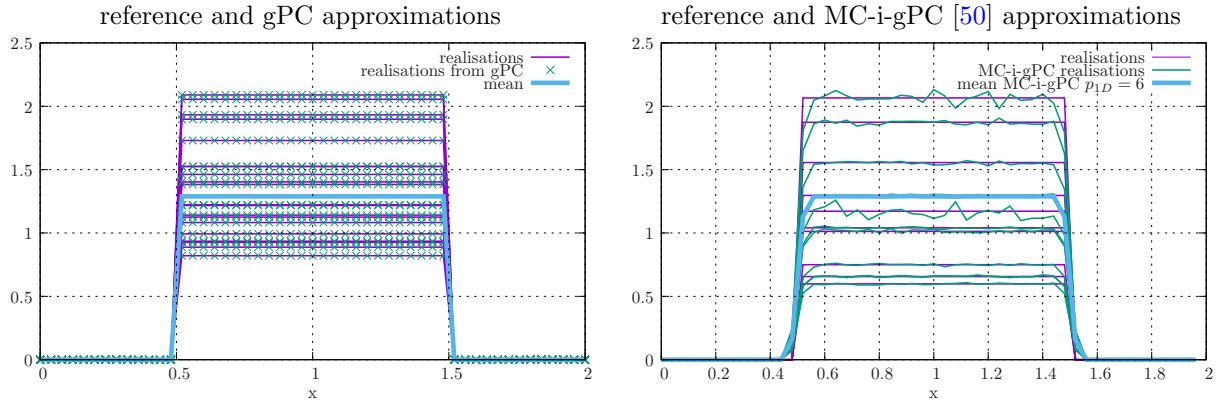


Figure 5: Mean and realisation comparisons between the analytical reference solution and a gPC reduced model ($p_{1D} = 10, P = 1000$) for time $t = 0.50$ for a semi-analytical resolution (left) and for an MC resolution (solver of [50]) (right) for the multidimensional test-problem of section 4.3.1.

The main trick in order to build an analytical solution comes from the fact we have $P_s(\omega, \omega') d\omega' = \delta_\omega(\omega')$: in this particular case u solution of (4) verifies⁷ $u(x, t, \omega, X) = u_0(x - v\omega t, \omega) e^{-v\sigma_a(X)t} = \delta_{x_0}(x - v\omega t) e^{-v\sigma_a(X)t}$, with $\sigma_a(X) = \sigma_t(X) - \sigma_s(X)$. As a consequence,

$$U(x, t, X) = \int u(x, t, \omega, X) d\omega = \frac{\mathbf{1}_{[x_0 - vt, x_0 + vt]}(x)}{vt} e^{-v\sigma_a(X)t}. \quad (33)$$

In practice, we choose

- $\bar{\sigma}_t = 1.0, \hat{\sigma}_t = 1.1$ so that there is a non-zero probability of having a multiplicative medium,
- $\bar{\sigma}_s = 0.0, \hat{\sigma}_s = 0.0$ so that the scattering cross-section is deterministic and X_2 has no influence,
- $\bar{\eta}_s = 1.0, \hat{\eta}_s = 0.5$ so that the density of matter is also uncertain.

With the above choice for σ_s , the test-case is in fact only 2D stochastic (as X_2 is in fact multiplied by zero). But still, we solve it in 3D stochastic dimension, on purpose, as if not knowing that parameter X_2 is not influent. We will come back to the reason why we do this when commenting on figure 7.

Figure 5 presents, at time $T = 0.50$, for several (randomly chosen) values of X :

- (left) the reference solution $x \rightarrow U(x, t^*, X)$ (given by (33)) together with its gPC approximations $x \rightarrow U^P(x, t^*, X)$ which, in the particular configuration of this section, is given by

$$U^P(x, t, X) = \frac{\mathbf{1}_{[x_0 - vt, x_0 + vt]}(x)}{vt} \sum_{k=0}^P U_k(t) \phi_k(X), \quad (34)$$

where $(U_k(t))_{k \in \{0, \dots, P\}}$ solves (29). System (29) is solved by applying the same methodology as in section 4.1.

- (right) the reference solution $x \rightarrow U(x, t^*, X)$ together with its MC-i-gPC approximations $x \rightarrow U_{MC}^P(x, t, X)$, obtained by solving directly (10) with an MC scheme (cf. [50]) with $N_{MC} = 8 \times 10^7$ MC particles.

The solutions $x \rightarrow U(x, t, X)$ and approximations $x \rightarrow U^P(x, t, X)$ have Heaviside shapes with fluctuating plateaus. As times passes, the plateaus' levels are lower but the Heaviside shapes are wider.

⁷It is built applying the characteristic method and intensively uses the fact that $\int P_s(\omega, \omega') u(\mathbf{x}, t, \omega') d\omega' = \int \delta_\omega(\omega') u(\mathbf{x}, t, \omega') d\omega' = u(\mathbf{x}, t, \omega)$.

The analytical and gPC curves (figure 5 left) present a *very good agreement*⁸. This may appear astonishing for the reader familiar with the approximation of uncertain *discontinuous* solutions (and the appearance of Gibbs phenomenon for gPC, see [41, 62, 34, 18, 15]). The gPC approximations of figure 5 do not seem to suffer the appearance of spurious modes: this is because the solution is discontinuous only with respect to the physical variable x , see (33). the smoothness hypothesis (9) is in fact always fulfilled: theorem 1 should apply. This will be verified numerically with the convergence study of figure 6. Before switching to figure 6, let us focus on figure 5 (right): it presents MC approximations of the gPC reduced model for $p_{1D} = 6$ in the same configuration: the MC noise dominates the gPC error (see the fluctuations around the plateaus) testifying of a gPC convergence rate faster than the MC numerical resolution one (see [50] for more details).

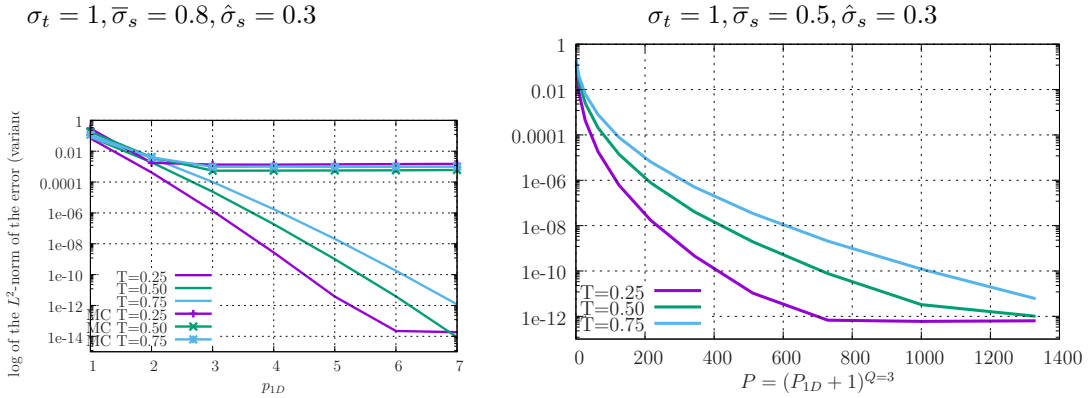


Figure 6: Left: convergence study with respect to p_{1D} obtained with the analytical solution (33), some gPC reduced models obtained from (34) and some MC approximations of (10), for several final times $T = 0.25, 0.50, 0.75$. Right: convergence study with respect to $P = (p_{1D} + 1)^{Q=3}$ obtained with the analytical solution (33) and some gPC reduced models obtained from (34) for several final times $T = 0.25, 0.50, 0.75$.

Figure 6 presents some convergence curves for the logarithm of the norm (15) of the error with respect to p_{1D} and with respect to $P = (p_{1D} + 1)^Q$ on this same problem for different times $t = 0.25, 0.50, 0.75$. The curves of figure 6 (left) allow numerically recovering the spectral convergence of the gPC approximation as predicted by theorem 1 (but in a multidimensional context): indeed, we have a linear curve $p_{1D} \rightarrow \log \left(\|u^{(p_{1D}+1)^Q}(t) - u(t)\|_{L^2(\mathcal{I} \times \Theta)}^2 \right)$. Second, we recover the fact that as t increases, the error of the gPC reduced model deteriorates⁹ as for a fixed p_{1D} , the error is bigger and bigger as time increases. On this same figure 6 (left) are displayed the same convergence study comparing the analytical solution (33) to the MC approximations of the gPC reduced model (10): the error stagnates around ≈ 0.005 which typically corresponds to the MC discretisation error ($\mathcal{O}(\frac{1}{\sqrt{N_{MC}}} \approx 0.005)$, with $N_{MC} = 8 \times 10^7$). For such MC discretisation, $P = 3$ is already below the MC numerical error. This fast gPC convergence is precious in an MC context, see [50]. The right picture of figure 6 presents the same study but with respect to P instead of p_{1D} . This picture attests that, in a multidimensional context, spectral convergence only holds with respect to p_{1D} and not P : the curves $P \rightarrow \log \left(\|u^P(t) - u(t)\|_{L^2(\mathcal{I} \times \Theta)}^2 \right)$ are sublinear. With this type of representation, it is easier having an idea of the increase in complexity of the gPC reduced model for a given accuracy (curse of dimensionality). Still, very good levels of accuracies can be reached for low polynomial orders in this case (errors below 10^{-4} as soon as $p_{1D} \geq 4$ and $P \geq (4 + 1)^3 = 125$).

⁸In a sense, this shows that the convergence is probably also pointwise in the random space for such smooth solutions. This fact has already been proven in [19] in a non-intrusive context.

⁹This echoes the previous discussions concerning the long-term behaviour of gPC but in a multidimensional context.

Let us finish this section by assuming that we would like to perform a sensitivity analysis: we would like to identify which of X_1 , X_2 or X_3 is the most influential on the total variability of the uncertain problem. For this, relative variance and Sobol indices are amongst the most relevant (but also costly) statistical tools, cf. [30]. In a gPC framework, the variance and the relative variances of each parameters, denoted respectively by $\mathbb{V}[U](\mathbf{x}, t)$ and $(\mathbb{V}_i[U](\mathbf{x}, t))_{i \in \{1,2,3,(1,2),(1,3),(2,3),(1,2,3)\}}$, can easily be approximated thanks to the gPC coefficients as

$$\begin{aligned}\mathbb{V}[U](\mathbf{x}, t) &\approx \mathbb{V}[U^P](\mathbf{x}, t) = \sum_{k=1}^P U_k^2(\mathbf{x}, t) = \sum_{s \in \mathcal{A}^{p_{1D}, Q} \setminus \{0\}} U_s^2(\mathbf{x}, t), \\ \mathbb{V}_i[U](\mathbf{x}, t) &\approx \mathbb{V}_i[U^P](\mathbf{x}, t) = \sum_{s \in \mathcal{S}_i} U_s^2(\mathbf{x}, t),\end{aligned}$$

where \mathcal{S}_i is a subset of $\mathcal{A}^{p_{1D}, Q}$ (see [6] for more details). So for all combinations i of the set $\{1, \dots, Q\}$,

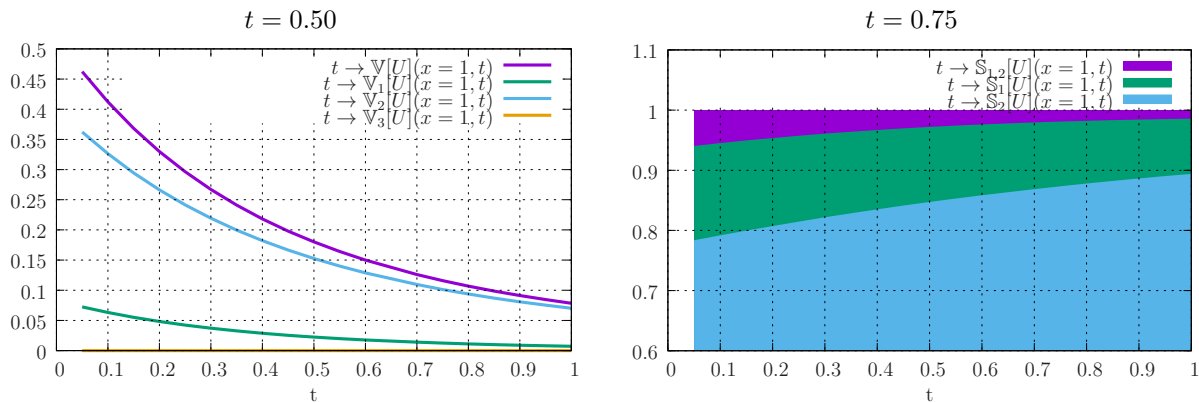


Figure 7: Left: variance and amount of variance explained by X_1, X_2, X_3 with respect to time for the multidimensional test-problem of section 4.3.1. Right: Sobol indices for X_1, X_2 and the couple (X_1, X_2) with respect to time for the multidimensional test-problem of section 4.3.1.

$\mathcal{S}_i \subset \mathcal{A}^{p_{1D}, Q}$. This means that from the spectral convergence¹⁰ of $\mathbb{V}[U^P]$ toward $\mathbb{V}[U]$, we can expect spectral convergence of every $\mathbb{V}_i[U^P]$ toward $\mathbb{V}_i[U]$. Figure 7 (left) presents the time evolutions of the relative variances at $x = 1$, i.e. $t \rightarrow \mathbb{V}_i[U^{p_{1D}=7}](x = 1, t)$, for $i \in \{1, 2, 3\}$. We can immediately recover the fact that X_3 is not influential during the whole time period: its relative variance is zero for all times $t \in [0, 1]$. This means we can reduce the dimensionality of our problem and neglect X_3 ¹¹: having access to such powerful statistical tools with a fast convergence is precious in industrial applications (more examples of this type can be found in [50]). On another hand, the same picture also allows identifying X_2 as the main parameter. Figure 7 (left) presents the time evolutions of the Sobol indices at $x = 1$. The Sobol indices and their respective gPC approximations are defined as follows: for all combinations i of the set $\{1, \dots, Q\}$, we have

$$\mathbb{S}_i[U](\mathbf{x}, t) = \frac{\mathbb{V}_i[U](\mathbf{x}, t)}{\mathbb{V}[U](\mathbf{x}, t)} \approx \mathbb{S}_i[U^P](\mathbf{x}, t) = \frac{\mathbb{V}_i[U^P](\mathbf{x}, t)}{\mathbb{V}[U^P](\mathbf{x}, t)}.$$

Figure 7 (right) presents three areas corresponding to the relative importance of parameters X_1, X_2 and their interactions (X_1, X_2) . Parameter X_2 , for early times $t \sim 0$, explains almost 79% of the variance. Parameter X_1 explains a little bit more than 14% of this same variance and the interactions of X_1, X_2 explains the remaining 6%. As time passes, X_1 and its interactions with X_2 are less and less influential.

¹⁰The L^2 -norm (15) ensures the convergence of the mean and the variance.

¹¹i.e. fix X_3 to its mean for example.

In the next subsection, we slightly revisit this same test-case and show that a small change in the uncertain set-up can lead to completely different behaviours.

4.3.2 A discontinuous 5D problem

In this section, we consider a modification of the previous multidimensional test-problem. The only difference with section 4.3.1 comes from the fact that X_3 now models some uncertainty in the initial condition rather than in the scattering cross-section. The initial condition is now a Dirac at $x_0(X) = x_0(X_3) = \bar{x}_0 + \hat{x}_0 X_3$ so that u_0 is given by $u_0(x, \omega, X) = \delta_{x_0(X)}(x) = \delta_0(x - x_0(X))$. In practice, we choose

- $\bar{\sigma}_t = 1.0, \hat{\sigma}_t = 1.1$ as in section 4.3.1.
- $\bar{\sigma}_s = 0.0, \hat{\sigma}_s = 0.0$ as in section 4.3.1 except that we now assume we know the scattering cross-section is zero whereas it was unknown in section 4.3.1.
- $\bar{x}_0 = 1.0, \hat{x}_0 = 0.1$ so that the uncertain initial condition is a Dirac translated along the x -axis.

We assume $X = (X_1, X_2, X_3)^t$ is a vector of independent uniform random variables on $[-1, 1]$. Once again, an analytical solution can be built and is given by $u(x, t, \omega, X) = u_0(x - v\omega t, \omega, X)e^{-v\sigma_a(X)t} = \delta_{x_0(X)}(x - v\omega t)e^{-v\sigma_a(X)t}$, with $\sigma_a(X) = \sigma_t(X) - \sigma_s(X)$. As a consequence,

$$U(x, t, X) = \frac{\mathbf{1}_{[x_0(X) - vt, x_0(X) + vt]}(x)}{vt} e^{-v\sigma_a(X)t}. \quad (35)$$

From the above expression, we can see that for this test-problem, both $x \rightarrow U(x, t, X)$ and $X \rightarrow U(x, t, X)$ can be discontinuous for (respectively) some values of (t, X) and of (x, t) .

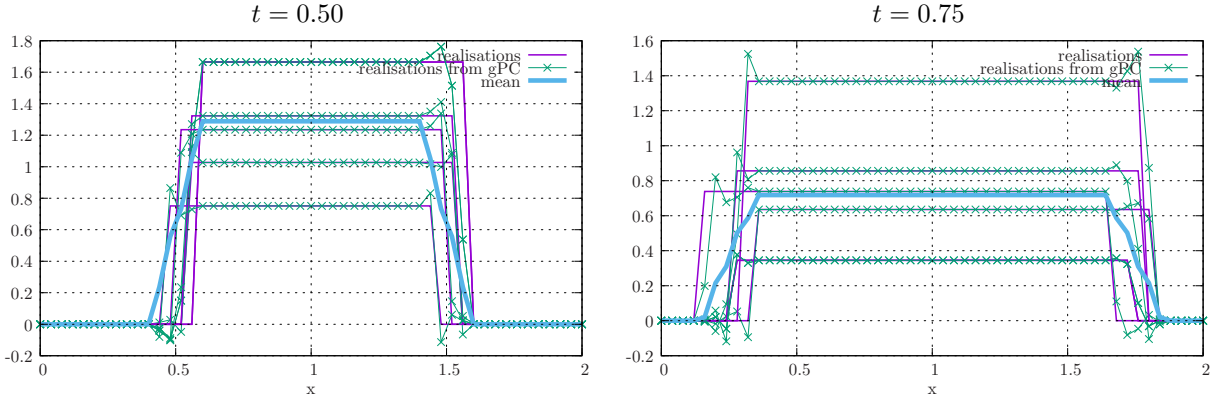


Figure 8: Mean and realisation comparisons between the analytical reference solution and a gPC reduced model ($p_{1D} = 10$, hence $P = 1331$) for times $t = 0.50$ (left), $t = 0.75$ (right) for the multidimensional test-problem of section 4.3.2.

Before commenting the figures of this section, let us briefly describe the numerical strategy to solve the gPC reduced model of this paragraph. For this, we intensively rely on the analogy between S_n models¹² and the gPC reduced model (10). In the particular case of this section, (10) resumes to

$$\partial_t \begin{pmatrix} u_0(x, t, \omega) \\ \dots \\ u_P(x, t, \omega) \end{pmatrix} + v \partial_x \omega \begin{pmatrix} u_0(x, t, \omega) \\ \dots \\ u_P(x, t, \omega) \end{pmatrix} + v \Sigma_a \begin{pmatrix} u_0(x, t, \omega) \\ \dots \\ u_P(x, t, \omega) \end{pmatrix} = 0,$$

¹²Note that this analogy between uncertainty quantification and kinetic theory is not original here, it has been highlighted in several works, see [33, 15, 49].

with Σ_a as in (29). We can apply the characteristic method to rewrite the previous system as

$$\partial_s \begin{pmatrix} u_0(x + v\omega s, s, \omega) \\ \dots \\ u_P(x + v\omega s, s, \omega) \end{pmatrix} + v\Sigma_a \begin{pmatrix} u_0(x + v\omega s, s, \omega) \\ \dots \\ u_P(x + v\omega s, s, \omega) \end{pmatrix} = 0,$$

which, once multiplied by the exponential of matrix $e^{v\Sigma_a s}$, resumes to

$$\partial_s \left[e^{v\Sigma_a s} \begin{pmatrix} u_0(x + v\omega s, s, \omega) \\ \dots \\ u_P(x + v\omega s, s, \omega) \end{pmatrix} \right] = 0.$$

If we now integrate the above expression on time step $[0, t]$ and introduce the vector of initial condition $(u_0(x, t = 0, \omega), \dots, u_P(x, t = 0, \omega))^t = (u_0^0(x, \omega), \dots, u_P^0(x, \omega))^t$, we get

$$\begin{pmatrix} u_0(x, t, \omega) \\ \dots \\ u_P(x, t, \omega) \end{pmatrix} = e^{-v\Sigma_a t} \begin{pmatrix} u_0^0(x - v\omega t, \omega) \\ \dots \\ u_P^0(x - v\omega t, \omega) \end{pmatrix}.$$

If we now are interested, as in the previous section, in vector $U(x, t) = (U_0(x, t), \dots, U_P(x, t))^t$, where $\forall k \in \{1, \dots, P\}, U_k(x, t) = \int u_k(x, t, \omega) d\omega$, then we have

$$\begin{pmatrix} U_0(x, t) \\ \dots \\ U_P(x, t) \end{pmatrix} = e^{-v\Sigma_a t} \begin{pmatrix} \int u_0^0(x - v\omega t, \omega) d\omega \\ \dots \\ \int u_P^0(x - v\omega t, \omega) d\omega \end{pmatrix}.$$

The exponential of matrix is equivalent to solving (29) with x, ω, t as parameters and is solved as in section 4.1. The integration of the initial condition $(u_0^0(x - v\omega t, \omega), \dots, u_P^0(x - v\omega t, \omega))^t$ with respect to ω for the positions of interest x is performed with a fine (100 points) Gauss-Legendre quadrature rule (close to an S_n model for a simple transport equation, see [4, 16, 12]).

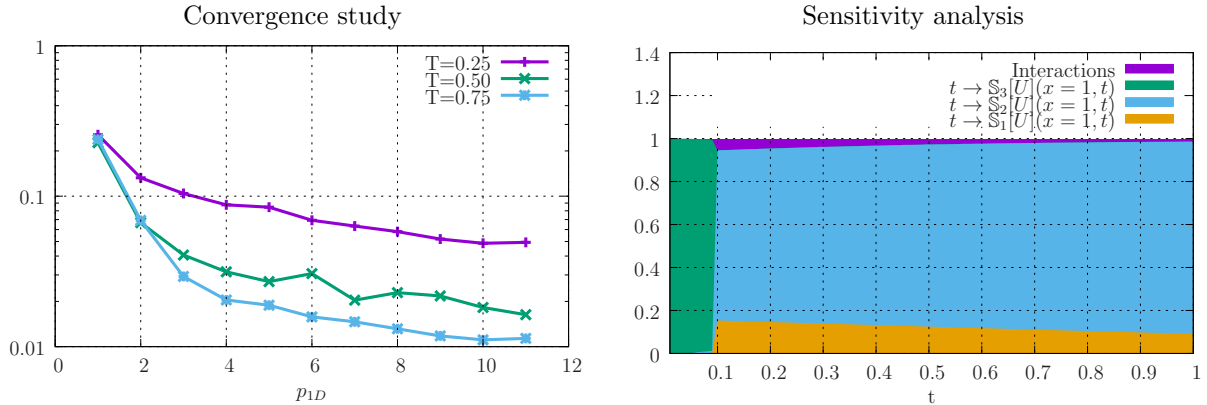


Figure 9: Right: convergence study with respect to p_{1D} obtained with the analytical solution (35) and some gPC reduced model for several final times $T = 0.25, 0.50, 0.75$. Right: sensitivity analysis, Sobol indices at $x = 1$ with respect to time.

Figure 8 presents spatial profiles of the reference solution $x \rightarrow U(x, t, X)$ and the gPC approximations $x \rightarrow U^P(x, t, X)$ obtained for $p_{1D} = 10$ (hence $P = 1331$) at two different times $t = 0.50, 0.75$ for 5 random realisations of X . The mean is also displayed. If we compare figure 8 and figure 5, the

profiles are similar except that the Heaviside shapes are now also translated along the x -axis. For this new test-problem, the gPC approximations do not anymore present the same levels of accuracy as encountered in section 4.3.1: the plateaus are well captured but some spurious oscillations are visible in the vicinities of the steep propagation fronts. Those spurious oscillations even lead to negative¹³ gPC reconstructions of the particle density U (see for example x around 0.5 in figure 8 (left)).

From (35), we can check that $X \rightarrow U(x, t, X)$ is only in¹⁴ H^0 , $\forall x \in [0, 2], \forall t > 0$. We are not in the condition of theorem 1. Figure 9 (left) presents some convergence studies for the logarithm of the L^2 -norm (given by (15)) of the error with respect to p_{1D} . In this case, the convergence is sublinear. One may notice that the curves present an improvement with respect to time: the curve for the earliest times are above the curves for the later ones. This is mainly due to the fact that with time, the spatial vicinities in which $X \rightarrow U(x, t, X)$ is discontinuous have less and less weight (remember norm (15) is integrated on the whole spatial domain) relatively to the vicinities presenting a smooth behaviour. This is confirmed by the sensitivity analysis of figure 9 (right): initially, the most influent parameter at $x = 1$ is X_3 : the green area takes the whole volume $[0, 0.1] \times [0, 1]$. But its importance suddenly drops after $t = 0.1$: after $t = 0.1$, the uncertainty in the propagation fronts do not have anymore impact at location $x = 1$ (remember that $\hat{x}_0 = 0.1$ and $[0, vt] = [0, 0.1]$ for $t \in [0, 0.1]$). After time $t = 0.1$, X_2 suddenly becomes the most influent parameter (blue area) at location $x = 1$, followed by X_1 (yellow area) and their global interactions (purple area). We insist that in practice, gPC based reduced model remain usable in such non-smooth context: care must only be taken to focus on smooth observables to obtain fast convergence rates.

5 Conclusion and open problems

In this paper, we considered the linear Boltzmann equation subject to uncertainties in the initial conditions and model parameters. In order to solve the underlying uncertain problem, we relied on moment theory and the construction of gPC based reduced models. The main result of this paper is the proof of the spectral convergence of the gPC based reduced models of the uncertain linear Boltzmann equation. The long-term behaviour of gPC reduced models have been theoretically put forward. The fast convergence of the approximations has also been recovered numerically. The numerical test-problems have been built to allow emphasizing the limitations of the theoretical result proved in this paper: some bounds are probably not optimal and theorem 1 may be pessimistic, especially for absorbing media. Still, this is encouraging as it implies the numerical convergence is even faster than the expected one (if, of course, care is taken to focus on smooth observables).

We finally would like to finish on few questions related to the ones discussed in this paper which we think may be of importance: first, despite the fast convergence rate of the reduced models, no positivity results on the uncertain density of particles is ensured. In practice, we did not encounter any problems as our computations are accurate enough and the robustness of our algorithm, see [50], does not rely on such condition. But this does not ensure positivity in future computations and may be problematic for some applications. The second problem is the curse of dimensionality and the fact the bigger the dimension Q of the uncertain vector X , the more coefficients are to be estimated. This point is addressed in [50]: the curse of dimensionality is partly compensated by an astute use of a Monte-Carlo scheme (less sensitive to the dimension) together with the ingredient of this paper. The last point we suggest to tackle is closely related to remark 3.2. There is a lack of theory for non uniform input random variables with respect to spectral convergence. In practice, spectral convergence is observed in many physical domains with respect to any input distribution. But the problem of having polynomials on unbounded domains (typically, we can not use a majoration such as (24) on an unbounded domain) makes the understanding more complex. Still, some results exists for L^∞ bounds in weighted spaces [40] and future effort will probably be carried on in this direction.

¹³cf. the previous discussions about the loss of positiveness on the fist test-problem of section 4.1.

¹⁴Remember that theorem 1 demands $u \in H^k$ with $k > 0$ for the results to apply.

References

- [1] Brunner T. A. and P. S. Brantley. An efficient, robust, domain-decomposition algorithm for particle Monte Carlo. *Journal of Computational Physics*, 228.10:3882–3890, 2009.
- [2] Milton Abramowitz and Irene A. Stegun. *Handbook of Mathematical Functions with Formulas, Graphs, and Mathematical Tables*. Dover, New York, ninth dover printing, tenth gpo printing edition, 1964.
- [3] R. Dautray and J.L. Lions. *Analyse mathématique et calcul numérique pour les sciences et les techniques*, volume tome 1-6. Masson, 1984.
- [4] Christian Aussourd. Styx: a multidimensional AMR S_N scheme. *Nuclear science and engineering*, 143(3):281–290, 2003.
- [5] G. Blatman and B. Sudret. Sparse Polynomial Chaos Expansions and Adaptive Stochastic Finite Elements using a Regression Approach. *C. R. Méc.*, 336:518–523, 2008.
- [6] G. Blatman and B. Sudret. Efficient computation of global sensitivity indices using sparse polynomial chaos expansions. *Rel. Eng. Syst. Saf.*, 95:1216–1229, 2010.
- [7] G. Blatman, B. Sudret, and M. Berveiller. Quasi-Random Numbers in Stochastic Finite Element Analysis. *Mech. Ind. proofs*, 8:289–297, 2007.
- [8] Emeric Brun, Stéphane Chauveau, and Fausto Malvagi. Patmos: A prototype monte carlo transport code to test high performance architectures. In Proceedings of International Conference on Mathematics & Computational Methods Applied to Nuclear Science & Engineering, Jeju, Korea, 2017.
- [9] Cacucci and Dan G. *Handbook of Nuclear Engineering*, volume 1. Springer Science & Business Media, 2010.
- [10] R.H. Cameron and W.T. Martin. The Orthogonal Development of Non-Linear Functionals in Series of Fourier-Hermite Functionals. *Annals of Math.*, 48:385–392, 1947.
- [11] Jose Antonio Carrillo and Mattia Zanella. Monte Carlo gPC methods for diffusive kinetic flocking models with uncertainties. 2019. preprint.
- [12] F. Chaland and G. Samba. Discrete ordinates method for the transport equation preserving one-dimensional spherical symmetry in two-dimensional cylindrical geometry. *Nuclear Science and Engineering*, 182(4):417–434, 2016.
- [13] T. Crestaux. Polynômes de Chaos pour la Propagation et la Quantification d’Incertitudes. Technical report, CEA, 2006.
- [14] M. K. Deb, I. M. Babuska, and J. T. Oden. Solution of Stochastic Partial Differential Equations using Galerkin Finite Element Techniques. *Comp. Meth. Appl. Mech. Engrg.*, 190:6359–6372, 2001.
- [15] Bruno Després, Gaël Poëtte, and Didier Lucor. *Robust Uncertainty Propagation in Systems of Conservation Laws with the Entropy Closure Method*, volume 92 of *Lecture Notes in Computational Science and Engineering*. Uncertainty Quantification in Computational Fluid Dynamics, 2013.
- [16] Qiang Du, Max D Gunzburger, and Lili Ju. Voronoi-based finite volume methods, optimal voronoi meshes, and pdes on the sphere. *Computer methods in applied mechanics and engineering*, 192(35):3933–3957, 2003.

- [17] J. Dufek and W. Gudowski. Stochastic approximation for Monte-Carlo Calculation of Steady-State Conditions in Thermal Reactors. *Nucl. Sci. Ener.*, 152:274–283, 2006.
- [18] Jakob Dürrwächter, Thomas Kuhn, Fabian Meyer, Louisa Schlachter, and Florian Schneider. A hyperbolicity-preserving discontinuous stochastic galerkin scheme for uncertain hyperbolic systems of equations. arXiv:1805.10177.
- [19] Ernst, Oliver G., Mugler, Antje, Starkloff, Hans-Jörg, and Ullmann, Elisabeth. On the convergence of generalized polynomial chaos expansions. *ESAIM: M2AN*, 46(2):317–339, 2012.
- [20] P. Frauenfelder, C. Schwab, and R.A. Todor. Finite Element for Elliptic Problems with Stochastic Coefficients. *Comp. Meth. Appl. Mech. Engrg.*, 194:205–228, 2004.
- [21] Walter Gautschi. *Orthogonal polynomials: applications and computation*, volume 5. Oxford University Press, 1996.
- [22] M. I. Gerritsma, J.-B. van der Steen, P. Vos, and G. E. Karniadakis. Time-dependent generalized polynomial chaos. *J. Comput. Physics*, pages 8333–8363, 2010.
- [23] R. G. Ghanem and J. Red-Horse. Propagation of Uncertainty in Complex Physical Systems using a Stochastic Finite Elements Approach. *Physica D*, 133:137–144, 1999.
- [24] R.G. Ghanem. Ingredients for a General Purpose Stochastic Finite Element Formulation. *Comp. Meth. Appl. Mech. Eng.*, 168:19–34, 1999.
- [25] R.G. Ghanem and P. Spanos. *Stochastic Finite Elements: a Spectral Approach*. Springer-Verlag, 1991.
- [26] R.G. Ghanem and P.D. Spanos. *Stochastic Finite Elements: a Spectral Approach*. Dover, 1991.
- [27] F. Golse and G. Allaire. *Transport et Diffusion*. 2015. Polycopié de cours.
- [28] Bal Guillaume. *Couplage d’équations et homogénéisation en transport neutronique*. PhD thesis, Université Paris 6, France, 1997.
- [29] T.D. Hien and M. Kleiber. Stochastic Finite Element Modeling in Linear Transient Heat Transfer. *Comp. Meth. Appl. Mech. Engrg.*, 144:111–124, 1997.
- [30] Bertrand Iooss and Paul Lemaître. *A Review on Global Sensitivity Analysis Methods*, pages 101–122. Dellino, Gabriella and Meloni, Carlo, Springer US, Boston, MA, 2015.
- [31] A. Keese. *A General Purpose Framework for Stochastic Finite Elements*. Ph. d. thesis, Mathematik und Informatik der Technischen Universität Braunschweig, 2004.
- [32] J. Kusch, G. W. Alldredge, and M. Frank. Maximum-principle-satisfying second-order intrusive polynomial moment scheme. *arXiv preprint arXiv:1712.06966*, 2017.
- [33] J. Kusch and M. Frank. Intrusive methods in uncertainty quantification and their connection to kinetic theory. *International Journal of Advances in Engineering Sciences and Applied Mathematics*, pages 1–16, 2018.
- [34] Jonas Kusch, Ryan G. McClarren, and Martin Frank. Filtered stochastic galerkin methods for hyperbolic equations. *J. Comput. Phys.*, 2018.
- [35] B. Lapeyre, E. Pardoux, and R. Sentis. *Méthodes de Monte Carlo pour les équations de transport et de diffusion*. Number 29 in Mathématiques & Applications. Springer-Verlag, 1998.

- [36] Coline Larmier, Andrea Zoia, Fausto Malvagi, Eric Dumonteil, and Alain Mazzolo. Monte carlo particle transport in random media: The effects of mixing statistics. *Journal of Quantitative Spectroscopy and Radiative Transfer*, 196:270 – 286, 2017.
- [37] O. Le Maitre, M. Reagan, H. Najm, R. Ghanem, and O. Knio. Multi-Resolution Analysis of Wiener-Type Uncertainty Propagation Schemes. *J. Comp. Phys.*, 197:502–531, 2004.
- [38] R. Lebrun and A. Dutfoy. A Generalization of the Nataf Transformation to Distributions with Elliptical Copula. *Prob. Eng. Mech.*, 24,2:172–178, 2009.
- [39] R. Lebrun and A. Dutfoy. An Innovating Analysis of the Nataf Transformation from the Copula viewpoint. *Prob. Eng. Mech.*, 24,3:312–320, 2009.
- [40] A.L. Levin and D.S. Lubinsky. Bounds for orthogonal polynomials for exponential weights. *Journal of Computational and Applied Mathematics*, 99(1):475 – 490, 1998. Proceeding of the VIIIth Symposium on Orthogonal Polynomials and Thier Application.
- [41] O. P. Le Maître and O. M. Knio. Uncertainty Propagation using Wiener-Haar Expansions. *J. Comp. Phys.*, 197:28–57, 2004.
- [42] O. P. Le Maître and O. M. Knio. A Stochastic Particle-Mesh Scheme for Uncertainty Propagation in Vortical Flows. *J. Comp. Phys.*, 226:645–671, 2007.
- [43] et al Martin, William R. Monte carlo photon transport on shared memory and distributed memory parallel processors. *International Journal of High Performance Computing Applications*, 1.3:57–74, 1987.
- [44] L. Mathelin and O. P. Le Maître. A Posteriori Error Analysis for Stochastic Finite Element Solutions of Fluid Flows with Parametric Uncertainties. *ECCOMAS CFD*, 2006.
- [45] M. Meyer and H.G. Matthies. Efficient model reduction in non-linear dynamics using the Karhunen-Loève expansion and dual-weighted-residual methods. *Comp. Meth. Appl. Mech. Eng.*, Informatikbericht 2003-08, TU Braunschweig, Germany, 2004.
- [46] Aaron J. Olson. Reduced-order monte carlo modeling of radiation transport in random media. Technical report, <https://digitalrepository.unm.edu/etds55>, 2016.
- [47] H. N. Najm O.P. Le Maître, O. M. Knio and R. G. Ghanem. A Stochastic Projection Method for Fluid Flow I: Basic Formulation. *J. Comp. Phys.*, 173:481–511, 2001.
- [48] B. Perthame. *Transport Equations in Biology*. Birkhauser Verlag, Basel Boston Berlin, 2000.
- [49] G. Poëtte. *Contribution to the mathematical and numerical analysis of uncertain systems of conservation laws and of the linear and nonlinear Boltzmann equation*. Habilitation à Diriger des Recherches, in english, Université de Bordeaux, école doctorale Mathématiques et Informatique, 2019.
- [50] Gaël Poëtte. A gPC-intrusive Monte-Carlo scheme for the resolution of the uncertain linear Boltzmann equation. *Journal of Computational Physics*, 385:135 – 162, 2019.
- [51] G. C. Pomraning. *The equations of radiation hydrodynamics*. Dover books on physics. Dover Publications, 1973.
- [52] Anil K Prinja. Notes on the lumped backward master equation for the neutron extinction/survival probability. Technical report, Los Alamos National Laboratory (United States). Funding organisation: DOE/LANL (United States), 2012.

- [53] Anil K. Prinja and Patrick O'Rourke. Transport in random media with inhomogeneous mixing statistics. *EPJ Web Conf., ICRS-13 & RPSD-2016, 13th International Conference on Radiation Shielding & 19th Topical Meeting of the Radiation Protection and Shielding Division of the American Nuclear Society - 2016*, 153, 5 2018.
- [54] L. Schlachter and F. Schneider. A hyperbolicity-preserving stochastic galerkin approximation for uncertain hyperbolic systems of equations. *arXiv preprint arXiv:1710.03587*, 2017.
- [55] P. Spanos and R. G. Ghanem. Stochastic Finite Element Expansion for Random Media. *ASCE J. Eng. Mech.*, 115(5):1035–1053, 1989.
- [56] B. Sudret and A. Der Kiureghian. Stochastic Finite Element Methods and Reliability - A State of the Art Report. Technical Report UCB/SEMM-2000/08, Department of civil and environmental engineering, University of California, Berkeley, 2000.
- [57] R. A. Todor and C. Schwab. Karhunen-Loève approximation of random fields by generalized fast multipole methods. *J. Comp. Phys.*, 217(1):100–122, 2006.
- [58] J. Tryoen, O. Le Maître, and A. Ern. Adaptive Anisotropic Stochastic Discretization Schemes for Uncertain Conservation Laws. *Proc. of ASME 2010, Third Joint US-European Fluids Engineering Summer Meeting*, 2010.
- [59] Xavier Valentin. *Analyse mathématique et numérique des modèles P_n pour la simulation de problèmes de transport de photons*. PhD thesis, Paris Saclay, 2015. Thèse de doctorat dirigée par Lafitte-Godillon, Pauline et Enaux, Cédric Mathématiques appliquées.
- [60] X. Wan and G.E. Karniadakis. Beyond Wiener-Askey Expansions: Handling Arbitrary PDFs. *SIAM J. Sci. Comp.*, 27(1-3), 2006.
- [61] X. Wan and G.E. Karniadakis. Long-Term Behavior of Polynomial Chaos in Stochastic Flow Simulations. *Comp. Meth. Appl. Mech. Engrg.*, 195:5582–5596, 2006.
- [62] X. Wan and G.E. Karniadakis. Multi-Element generalized Polynomial Chaos for Arbitrary Probability Measures. *SIAM J. Sci. Comp.*, 28(3):901–928, 2006.
- [63] N. Wiener. The Homogeneous Chaos. *Amer. J. Math.*, 60:897–936, 1938.
- [64] B.R. Wienke. Transport equations in moving material part i: Neutrons and photons. *Progress in Nuclear Energy*, 46(1):13–55, 2005.
- [65] J. A. S. Witteveen and H. Bijl. An Unsteady Adaptive Stochastic Finite Elements Formulation for Rigid-Body Fluid-Structure Interaction. *Comp. and Struct.*, 2008.
- [66] D. Xiu and G.E. Karniadakis. Modeling Uncertainty in Flow Simulations via generalized Polynomial Chaos. *Comp. Meth. Appl. Mech. Engrg.*, 187:137–167, 2003.